

MASTER

Water and ion dynamics in thin water films on LiCl surfaces a molecular dynamics study

Boomstra, M.W.

Award date:
2020

[Link to publication](#)

Disclaimer

This document contains a student thesis (bachelor's or master's), as authored by a student at Eindhoven University of Technology. Student theses are made available in the TU/e repository upon obtaining the required degree. The grade received is not published on the document as presented in the repository. The required complexity or quality of research of student theses may vary by program, and the required minimum study period may vary in duration.

General rights

Copyright and moral rights for the publications made accessible in the public portal are retained by the authors and/or other copyright owners and it is a condition of accessing publications that users recognise and abide by the legal requirements associated with these rights.

- Users may download and print one copy of any publication from the public portal for the purpose of private study or research.
- You may not further distribute the material or use it for any profit-making activity or commercial gain



Technische Universiteit
Eindhoven
University of Technology

Department of Applied Physics
TPM & TPS Research Groups

Water and Ion Dynamics in Thin Water Films on LiCl Surfaces

A Molecular Dynamics Study

Maarten Willem Boomstra

Supervisors:
dr. ir. H.P. Huinink
dr. A.V. Lyulin

Final version

Eindhoven, April 2020

Abstract

ThermoChemical Materials (TCMs) can be used to produce heat batteries for seasonal heat storage. A promising category of TCMs are salt hydrates. These release heat during hydration and can be charged by heating them, resulting in dehydration.

Previous experimental studies on these materials showed that the transition from the anhydrous crystal to a hydrated crystal takes place via an intermediate step. Water vapour is attracted to the salt and forms a thin film into which salt ions dissolve and subsequently recrystallisation into the hydrated crystal takes place.

The dissolution of LiCl into films was studied by molecular-dynamics simulations. First, force fields available from literature were benchmarked. Subsequently, thin films containing various amounts of water were studied, focusing on the interactions they had with the salt crystal. The main results were:

- The self-diffusion of water in films on the surface of LiCl crystals increases with the amount of water.
- Water molecules at the crystal surface have a preferred orientation, with the oxygen atom being closest to the surface and near a lithium ion.
- The time needed to dissolve ions depends on the surface geometry of the salt. No dissolution was observed on a flat surface within 50 ns. Stub systems showed the fastest dissolution, Ridge was slower and Dent the slowest.
- The time needed to dissolve ions decreases with the amount of water in the films.
- The occupancy of hydration shells changes with the total amount of water.
- Self-diffusion of water is lowered by the presence of ions in the water film.

The results provide more detailed information than can be experimentally gathered, contributing to the overall understanding of the hydration process of this TCM. For future study, it is advised to also look into the recrystallisation and the dehydration processes.

Potassium carbonate is a promising material for use in heat batteries, but very little force field data is available in literature. It is therefore recommended to make a multi-scale study of this salt hydrate.

Preface

When looking for a Masters graduation project, I had two wishes: a computational project and a subject related to the energy transition. These were both perfectly met by the topic of this thesis, molecular-dynamics simulations of the ThermoChemical Material lithium chloride and its interaction with water.

Working on this project has been instructive as well as enjoyable, for which I would like to thank my supervisors Alexey Lyulin and Henk Huinink. Thank you both for your guidance and the interesting discussions.

Furthermore, most simulations in this project were run on the national supercomputer Cartesius with the support of SURF Cooperative. Without these resources, running all simulations would not have been possible.

Contents

Contents	vii
1 Introduction	1
2 Simulation Methods and Models	5
2.1 Crystal Structure of Anhydrous Lithium Chloride	5
2.2 Molecular Dynamics	6
2.2.1 Integration Algorithm	6
2.2.2 Thermostat and Barostat	6
2.2.3 Periodic Boundary Conditions and Verlet Lists	7
2.3 Force Fields	8
2.3.1 Inter-molecular forces	8
2.3.2 Water Models and <i>SHAKE</i>	10
2.3.3 Choice of Input Parameters	11
2.4 System Initialisation and Equilibration	12
2.4.1 Surface configurations	12
2.5 Equilibration	14
2.6 Water Adding	16
2.7 Computational Resources and Software	16
3 Results & Discussion	17
3.1 Benchmarking	17
3.2 Water Structure and Dynamics at a Flat Surface	20
3.2.1 Translational self-diffusion of water	20

CONTENTS

3.2.2	Orientation of water molecules	24
3.3	Dissolution at Surfaces of Different Geometry	28
3.3.1	Dissolution rate for increasing water counts	28
3.3.2	Order of ions dissolving	31
3.3.3	Hydration Shells	33
3.3.4	Mobility of Water and Ions in Solution	34
4	Conclusions and Outlook	37
4.1	Conclusions	37
4.2	Outlook	39
Bibliography		41
A Appendices		45
A.1	Input parameters available from literature	45
A.2	Water adding	46
A.3	Additional measurements of dissolution	47
A.3.1	Dissolution quantified for different geometries into a film with 512 water molecules	47
A.3.2	Dissolution visualised for different geometries into a film with 512 water molecules	48
A.4	LAMMPS input file	49
A.5	MATLAB scripts	51
A.5.1	Import script	51
A.5.2	Script to Measure Orientation of Water Molecules	52

Chapter 1

Introduction

In the current environmental crisis, alternatives for fossil fuels are needed. A sustainable way of heating houses and offices is by use of heat batteries. In these batteries, the surplus of heat during summer (period E in Figure 1.1) can be stored and then used during cold months (period H).

Three working principles for heat batteries are sensible, latent and thermochemical heat storage. Sensible heat storage makes use of the heat capacity of a material, simply heating it up to store heat. For latent heat storage, Phase Change Materials (PCM) are used and heat is stored and recovered by transition between e.g. solid and liquid phase. [1] Downsides of these materials are the limited amount of heat that can be stored per kg of material and the loss of heat in time.

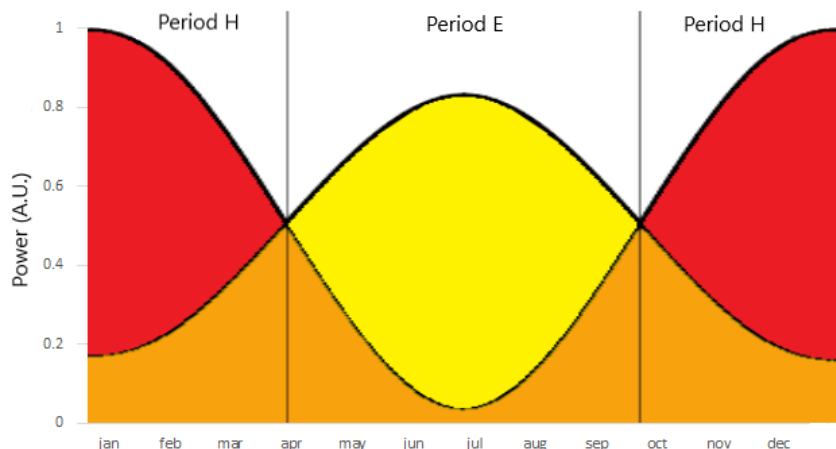


Figure 1.1: Schematic drawing of solar irradiation (yellow) and heat consumption (red) over a year, adapted from [2]

A ThermoChemical Material (TCM) is a material which releases heat when absorbing a reactive gas. [3] The opposite process, the release of reactive gas, is endothermic. There are a few possible reactive gasses, like water, ethanol and ammonia, all in vapour phase. For housing, water is the safest and most compatible with Dutch safety regulations. [4] This brings us to the materials of interest in this project, salt hydrates.

Recently, TU/e and TNO jointly developed a functioning heat battery based on thermochemical heat storage. This battery uses potassium carbonate as storage material. By bringing it into contact with water vapour, a hydrate is formed and heat is released. The battery can be charged

by heating up the hydrate and thus separating water from the salt. Figure 1.2 shows the complete closed system in which heat from e.g. solar panels can be stored and by which tap-water for showering can be heated. The reactor containing the actual salt hydrate is in the middle. On the left is a vessel for storing water, keeping the system closed. On the right is a boiler.

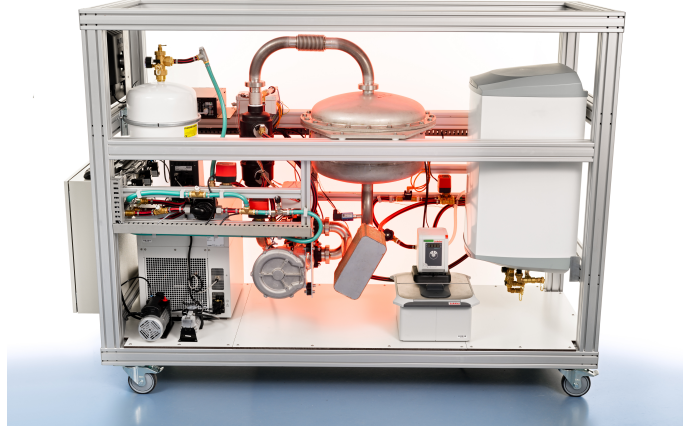
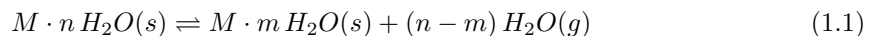
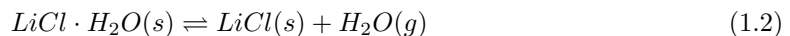


Figure 1.2: Heat battery by TU/e and TNO [5]

For salt hydrates in general, in which transitions between higher and lower hydrates are possible, the hydration and dehydration processes are [6]:



in which $M \cdot n H_2O(s)$ is the higher hydrate, called thus because of the higher amount of water molecules per unit of salt ($n > m$). The water that is absorbed or released is present as vapour (gaseous phase (g)) and the salts are solid (s). In the specific case of the anhydrate and monohydrate of lithium chloride, which will be studied hereafter, we have:



Much experimental research was done on TCM. This gave information on the conditions under which the (de)hydration processes take place and the behaviour of the materials at the macroscopic scale. [1] For further fundamental understanding of TCM, information is wanted on the molecular level. Techniques like X-Ray Diffraction spectroscopy (XRD) provide insight into structure, but of the beginning and end products, not during the (de)hydration process itself.

Atomistic molecular-dynamics (MD) is a useful computational tool to learn more about the dynamics on the atomic scale. By use of suitable potential models (force fields), the movements of atoms can be simulated. It is more suitable than, for example, Monte Carlo or coarse-grained simulations because the topic of interest is the detailed interactions between water molecules and ions and their behaviour in time, exactly what MD provides.

From a macroscopic viewpoint, it could be said that addition of water to dry lithium chloride will produce lithium chloride monohydrate, see Figure 1.3. However, Sögütoglu et al. [7] concluded from experiments that there is an intermediate step in this phase transition: the salt first dissolves in a film of water and subsequently recrystallises in the monohydrate form, shown schematically in Figure 1.4.

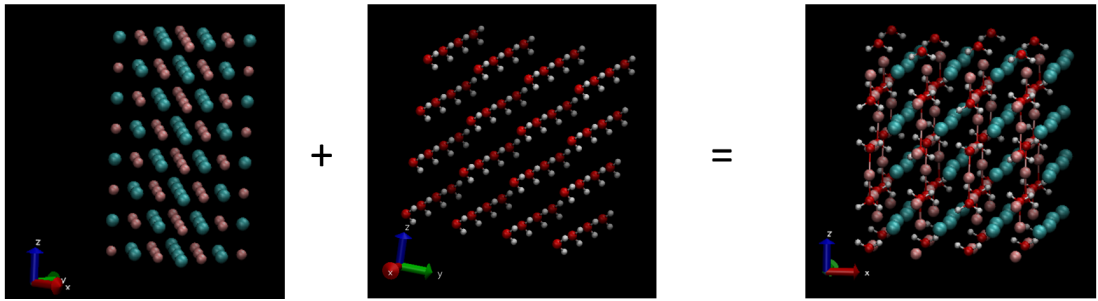


Figure 1.3: Adding water (centre) to LiCl anhydrate (left) gives monohydrate (right). Li pink, Cl blue, H_2O red and white. These pictures are made with Visual Molecular Dynamics (VMD) [8].

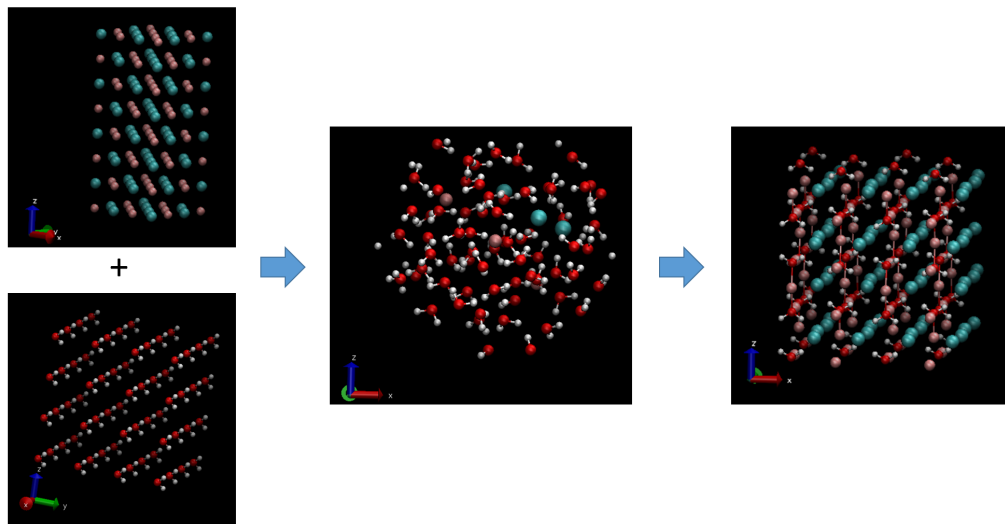


Figure 1.4: The anhydrate dissolves in water and then recrystallises as monohydrate. In the centre a solution of lithium and chloride ions in water is depicted, the rest is the same as in Figure 1.3

Salt hydration and dehydration always attracted attention. Multiple studies were done on NaCl and its interaction with water, both using simulations [9][10] and experiments [11][12]. Bahadur et al. [9] studied the influence of lattice defects on dissolution using classical MD. Liu et al. [10] analysed the structure and dynamics in a water film on NaCl with *ab initio* MD. Foster and Ewing [11] used infrared spectroscopy to study the structure of water films. Bruzewicz et al. [12] investigated reversible water uptake on nanoparticles of NaCl by use of atomic force microscopy.

In the present thesis Lithium Chloride, LiCl, is chosen to look into because it is a monovalent ionic crystal, which can be well described by simple force fields. Data is available to start simulations with [13]. Since LiCl and NaCl are similar substances with equal crystal shapes, results from the previous studies can be used for comparison. This makes LiCl a good starting point for MD study of salt hydrates.

MD studies of LiCl have been done by others, e.g. by Heinzinger and Vogel [14] who simulated LiCl already in solution. Fukushima et al. [15] simulated the dissolution of nanocrystals for short times. Du and Miller [16] found that there is a preference for Li to be released from the crystal, in contradiction to the findings by Fukushima et al. A more complete picture of the dissolution of LiCl is wanted, this is what we focus on in the present study.

LiCl, like many other salts, attracts water vapour from its surroundings. This attraction is in fact so strong, that the water forms a thin film on the LiCl surface into which salt ions dissolve, see Figure 1.5. This is called deliquescence [7] and has not been previously studied with MD.

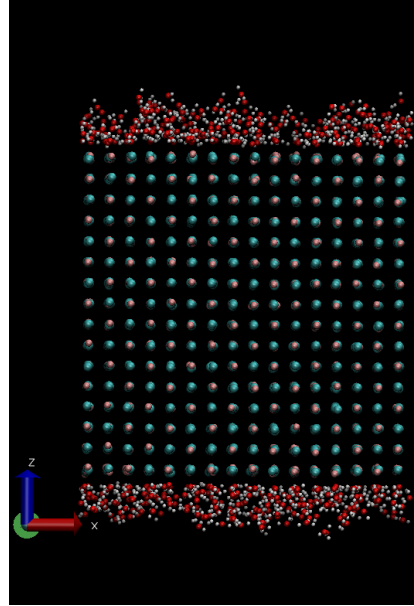


Figure 1.5: *LiCl crystal with water films on the surfaces. These films were formed by attraction of water vapour towards the salt. The simulation box is 42 by 42 Å wide and 160 Å high.*

The aim of this thesis is to learn more about the first step in the hydration process, the deliquescence. The main question to be answered is: how exactly does the dissolution of LiCl into these thin water films take place on the atomic scale? As already stated, MD is the most suitable method of simulation. Different force fields were tested after which simulations were run. The results were then post-processed to gain insight into the dissolution process.

Chapter 2

Simulation Methods and Models

The crystal structure of the salt under study, lithium chloride, will be shortly discussed. Subsequently, an introduction to the molecular-dynamics simulation technique will be given. Finally, the models used and the way they were implemented will be treated.

2.1 Crystal Structure of Anhydrous Lithium Chloride

Lithium Chloride, in solid state, is an ionic crystal. The structure of a crystal is defined by its unit cell, the smallest group of atoms that repeats itself 3 dimensionally. Figure 2.1 shows the unit cell of anhydrous LiCl.

A unit cell can be defined by 6 dimensions, the basis vectors \vec{a} , \vec{b} and \vec{c} and the angles between these vectors α , β and γ . These are shown in Figure 2.2.

The dimensions of the LiCl unit cells were downloaded from the American Mineralogist Crystal Structure Database [17], based on data from X-Ray Diffraction measurements by Wyckoff [18].

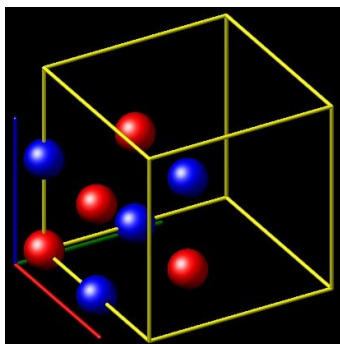


Figure 2.1: Unit cell of anhydrous LiCl, visualised by LAMMPS. Li red, Cl blue. The sizes of the balls do not correspond to the radii of lithium and chloride ions, which are unequal. $a=b=c=5.13 \text{ \AA}$. $\alpha = \beta = \gamma = 90^\circ$.

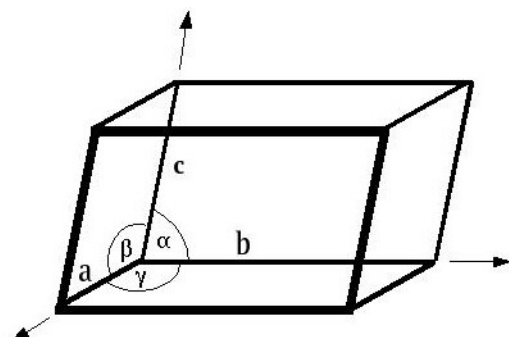


Figure 2.2: Dimensions of a unit cell [19]

2.2 Molecular Dynamics

As the name already says, molecular-dynamics (MD) is a tool to study the movements of molecules due to the forces between them. The basis of MD lies in Newton's second law, $\vec{F} = m \cdot \ddot{\vec{r}}$ with F [N] the force acting on the particle under consideration, m [kg] the particle's mass and $\ddot{\vec{r}}$ [m/s^2] its acceleration.

All simulations done for this study were run with the Large-scale Atomic/Molecular Massively Parallel Simulator (LAMMPS) by Sandia National Laboratories [20].

2.2.1 Integration Algorithm

When the forces between particles are known, so are their accelerations and by double integration their trajectories. A finite difference scheme is needed for obtaining particle trajectories by integration. A well-known method is Verlet integration [21]. This can be derived by a Taylor expansion of the position of an atom [22]:

$$\vec{r}(t + \delta t) = \vec{r}(t) + \delta t \vec{v}(t) + \frac{1}{2} \delta t^2 \vec{a}(t) + \dots \quad (2.1)$$

$$\vec{r}(t - \delta t) = \vec{r}(t) - \delta t \vec{v}(t) + \frac{1}{2} \delta t^2 \vec{a}(t) - \dots \quad (2.2)$$

giving by addition

$$\vec{r}(t + \delta t) = 2\vec{r}(t) - \vec{r}(t - \delta t) + \delta t^2 \vec{a}(t) \quad (2.3)$$

The most widely used method of time-integration is velocity-Verlet, which is shown to be reliable [23]. It differs from the original method [21] by explicit calculation of the velocity:

$$\vec{v}(t + \delta t) = \vec{v}(t) + \frac{1}{2} \delta t (\vec{a}(t + \delta t) + \vec{a}(t)) \quad (2.4)$$

This velocity-Verlet algorithm is also the one used for this study.

2.2.2 Thermostat and Barostat

The equations of motion described in the previous section apply to particles of which the total energy remains constant, a so called NVE ensemble, where N is the constant total amount of particles, V the constant volume of the simulation box and E the constant internal energy.

A system with constant temperature (but fluctuating energy) and constant volume and amount of particles defines the canonical or NVT ensemble. The temperature T is controlled by a thermostat, which also provides the possibility of ramping the temperature to a desired value. This is done by letting heat flow into and out of the simulation box from a heat bath, extending the equations of motion with an extra degree of freedom for the heat bath as compared to the NVE ensemble. The NVT integration algorithm implemented in the software used in this study makes use of thermostats of the Nosé-Hoover type and uses equations of motion described by Shinoda et al. [24] and is of the type described by Tuckerman et al. [25]. The proposed thermostat damping time by the LAMMPS manual is 100 time-steps.

The volume can also be made variable, making use of extension of the equations of motion with a "piston mass" term [22]. Now the pressure P can be ramped to a desired value as well, by a

barostat. By combining this with a thermostat, we can simulate an NPT ensemble. In this study the barostat used is also of the Nose-Hoover type [24] [25]. The thermostat for pressure ramping is another than that of the temperature ramping. The proposed damping time for this thermostat is 1000 time-steps.

When simulating crystals, a so called $N\sigma T$ ensemble is preferred, as described first by Parrinello and Rahman [26]. In LAMMPS an $N\sigma T$ ensemble can be simulated making use of the *NPT* function with the additional command *tri*. This way, the box dimensions are given freedom to vary independently while the external normal stress is kept constant.

2.2.3 Periodic Boundary Conditions and Verlet Lists

In MD, often Periodic Boundary Conditions (PBC) are used. A 2D illustration [22] of this is shown in Figure 2.3. The actual simulation box is in the centre in grey. Because of the PBC, it can be viewed as being surrounded by copies of itself. Particle 1, which moves upwards beyond the boundary moves back into the simulation box from below, exactly the same way as it moves into copy C and all other copies. One of the advantages of using PBC is that, with 3D PBC, materials can be simulated as though they are in bulk. This is under the condition that the typical physical length scale of the problem is below the box size. Simulation boxes that are too small can, for example, cause unwanted effects on particle clustering.

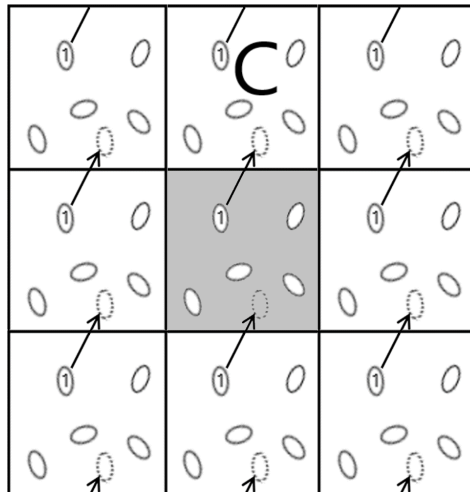


Figure 2.3: 2D illustration of PBC, adapted from [22]. A cell with PBC can be thought of as being surrounded by copies of itself.

Another widely used technique is the use of Verlet neighbour lists [21]. Forces between particles are often set to zero beyond a cut-off radius r_c , as will be further discussed in Section 2.3.1. For each particle i , a list can be made of all particles that are within r_c and therefore exert a non-zero force on i . Per time instance, these are all the particles of interest for calculation of forces. By expanding the list with particles of which $r_c < r < r_V$ a Verlet list is obtained, as shown in Figure 2.4 [23]. This list can be used for multiple time-steps because the particles that move into the inner sphere with radius r_c are already known from the Verlet list as long as $v \cdot \Delta t < (r_V - r_c)$, with v the average velocity of a particle relative to particle i and Δt the time for which the Verlet list is used. This technique speeds up simulations significantly.

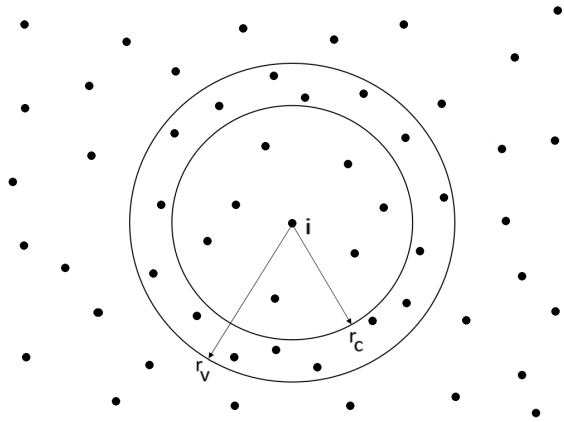


Figure 2.4: Principle of a Verlet list, picture adapted from [23]. A Verlet list contains all particles within radius r_v . The cut-off radius r_c is the maximum distance at which particle i interacts with other particles. Within a certain time interval, the Verlet list contains all particles that can move into radius r_c making it unnecessary to consider particles not on the list.

2.3 Force Fields

A combination of potentials describing forces between particles and e.g. bonds or dihedrals within molecules is called a force field.

Under the assumption that the force between two particles is not influenced by the presence of other particles, the force is described by a so called two body potential. Apart from for metals, pair potentials are widely used in MD and give results agreeing well with experiments. The force acting on a particle can be calculated from the potential: $\vec{F}_i = -\nabla V_i$, where V_i [J] is the sum of the atom-atom interaction potentials with all surrounding particles $V_i = \sum_{j \neq i} V_{ij}$.

2.3.1 Inter-molecular forces

The simulations presented in this thesis are all based on the combination of the Lennard-Jones (LJ) potential [27] and Coulombic interaction.

As Verlet [21] showed, the LJ potential gives results that agree well with experimental data of particles without electrical charge, in his case argon atoms. The well-accepted model describing both the van der Waals attractive force and the repulsive force that prevents particles from merging is based on the LJ interaction potential described as:

$$V_{LJ} = 4\epsilon \left[\left(\frac{\sigma}{r} \right)^{12} - \left(\frac{\sigma}{r} \right)^6 \right] \quad r < r_c, \quad (2.5)$$

with V_{LJ} [kJ] the potential, ϵ [kJ] the depth of the well, r [\AA] the distance between the particles and σ [\AA] the distance at which the potential is zero. Every atom species has its own values of these parameters. These are valid for interactions between atoms of the same type. For interactions between unlike species, the Lorentz-Berthelot rules are used:

$$\begin{aligned} \sigma_{ij} &= \frac{\sigma_i + \sigma_j}{2} \\ \epsilon_{ij} &= \sqrt{\epsilon_i \cdot \epsilon_j} \end{aligned} \quad (2.6)$$

Figure 2.5 shows plots of the LJ potential, the Coulombic potential and their combination. As can be seen, the LJ potential reaches its asymptotic value of 0 quite quickly. It is therefore customary to cut off the potential at $r_c = 2.5 \cdot \sigma$, taking $V = 0$ for $r \geq r_c$

The Coulombic potential between charged particles is, in SI units:

$$V_{Coul} = \frac{1}{4\pi\epsilon_0} \frac{q_1 \cdot q_2}{r}, \quad (2.7)$$

with V_{Coul} [kJ] the potential, q_1 and q_2 [C] the electric charges of the particles and ϵ_0 [F/m] the vacuum permittivity. Since it is inversely proportional to the distance, it approaches zero much more slowly. When using a cut off radius, this would need to be very large to prevent large errors and these large cut offs are not possible in systems with periodic boundaries. Another option is to make use of Ewald summation [28] or a faster alternative, the Particle-Particle Particle-Mesh (PPPM) method. [29]

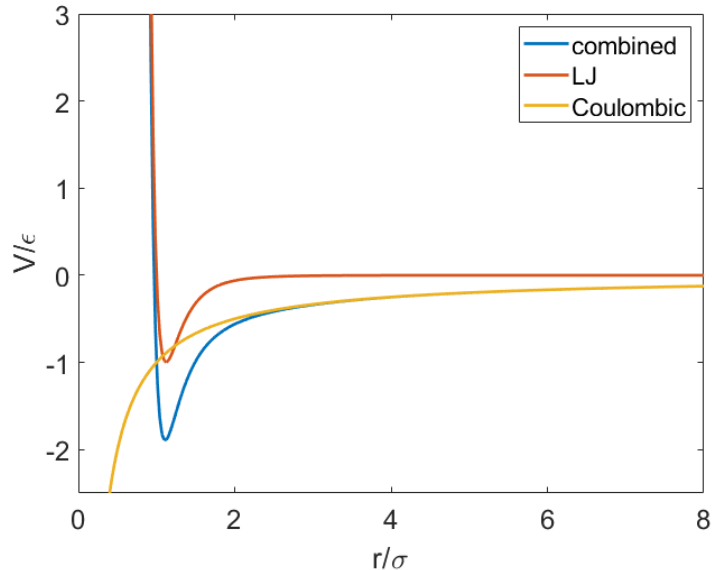


Figure 2.5: Lennard-Jones potential, Coulombic potential and both combined. The following values were assigned: $\epsilon = 1 \text{ kJ}$, $\sigma = 1 \text{ \AA}$ and $\frac{q_1 \cdot q_2}{4\pi\epsilon_0} = -1 \text{ \AA} \cdot \text{kJ}$. The Lennard-Jones potential reaches $V = 0$ around $r = 2.5 \sigma$ while this takes much longer for the Coulombic potential and the combination. The Coulombic potential gets very large negative values at shorter distances, resulting in a lower minimum value for the combination.

2.3.2 Water Models and *SHAKE*

Since water molecules are strongly dipolar, their simulation is not straightforward. Many water models have been developed, a large part of which make use of LJ-Coulombic potentials. These differ in values assigned to electrical charge, LJ parameters, characteristics of the O-H bonds and relative positions of the atoms and hereby the H-O-H angle. Examples of widely known water models are, amongst others:

- SPC/E: Extended Single Point Charge [30]
- TIP3P: Transferable Inter-molecular Potential with 3 Points [31]
- TIP4P-Ew: TIP with 4 Points for use with Ewald techniques [32]

Figure 2.6 illustrates the TIP4P model. In all three models mentioned, the LJ parameters ϵ and σ are only set for the oxygen atom, the hydrogen atoms have no LJ interaction with other particles. The length of the OH bonds is r_{OH} and the angle between them θ_{HOH} . Electric charges of atoms are usually given in partial charges, non-integer multiples of e , the charge of a proton $1.602 \cdot 10^{-19}$ C. In the SPC/E and TIP3P models the oxygen atom has a partial charge of $-q$ and because a water molecule is electrically neutral, the hydrogen atoms each have partial charge $-q/2$. In the TIP4P model, charge $-q$ is set at a lower position instead of at the oxygen atom.

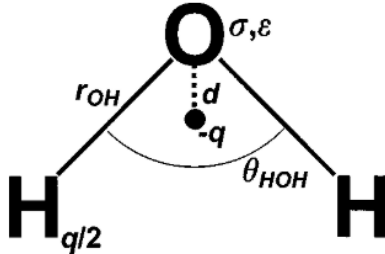


Figure 2.6: Illustration of the TIP4P water model [32]

The LAMMPS manual [33] recommends defining both bonds and angle by a harmonic potential,

$$E_b = K_b \cdot (r - r_0)^2 \quad (2.8)$$

and

$$E_a = K_a \cdot (\theta - \theta_0)^2, \quad (2.9)$$

with r_0 [Å] and θ_0 [degrees] the equilibrium values of bond length and angle respectively and K_b [kcal/(mol·Å²)] and K_a [kcal/mol] pre-factors defining strength of the potentials. In practice this was only used during minimisation, see section 2.4. During all simulations the bonds and angles were kept rigid by use of the *SHAKE* algorithm [34].

When the bond lengths and angles in water molecules vary, this adds additional degrees of freedom to the equations of motion. Hereby the integration algorithm of the thermostat and/or barostat requires more computation. The *SHAKE* algorithm [34] keeps the bond lengths and angle constant, resulting in much faster simulations.

2.3.3 Choice of Input Parameters

Depending on what property is of interest in a simulation, e.g. diffusion, freezing point or interaction with ions, different water models give the most accurate results. The same holds for the salt, different LJ parameters ϵ and σ result in different properties of the salt. When studying e.g. solubility, certain values of these parameters will give the best results, closest to experimental data. For e.g. an accurate value of the melting point of the salt, other ϵ and σ are best suited. Furthermore, when simulations including water are run, the water model used also influences the choice of the LJ parameters of the salt.

In this study, force field parameters were taken from literature. For different inputs, the stability of the anhydrous lithium chloride and the monohydrate crystals were checked. Quantitative results of this benchmarking process are discussed in Chapter 3, along with the reasoning to choose the SPC/E water model to work further with.

The full set of input parameters for the particles is:

Table 2.1: **LJ parameters, partial charges and masses per atom type** [13]

	ϵ (kJ/mol)	σ (Å)	q (e)	m (g/mol)
Li	1.4	1.41	+1	6.941
Cl	0.054	4.83	-1	35.453
H	0.000	0.000	+0.4236	1.00794
O	0.65	3.166	-0.8472	15.9994

with $1\text{\AA} = 10^{-10}\text{m}$ and $e = 1.602 \cdot 10^{-19}\text{C}$. As discussed in Section 2.3.1, the LJ interactions between unlike species are calculated using the Lorentz-Berthelot rules.

The parameters of the angle and bond potentials of the SPC/E model as implemented in LAMMPS are:

Table 2.2: **Parameter values of the harmonic bond and angle potentials** [30][33]

K_a (kJ/mol)	418.4
K_b (kJ/(mol·Å ²))	4184
θ_0 (degrees)	109.47
r_0 (Å)	1.0

Other input parameters were:

- For all simulations the time-step was set to 1.0 fs.
- The cut-off radius r_c used was 11.0 Å,
- The thickness of the Verlet shell $r_V - r_c$ was 2.0 Å.
- The damping time of the thermostat was set to 100 fs.
- The damping time of the barostat was set to 1 ps.

2.4 System Initialisation and Equilibration

Before MD simulations of a system of particles can run, the initial positions, velocities and masses need to be specified. In the cases of an ionic crystal and water, also the electrical charges need to be given as input. The parameters for the potentials describing the forces were discussed in Section 2.3.3

The initial positions of the ions in the salt crystal were taken from a Crystallographic Information File (.cif) containing the data of a unit cell from X-Ray Diffraction measurements [18]. These can be fed to LAMMPS in two ways, either by converting and supplementing the data to make a LAMMPS data file, or by manually defining a lattice and placing ions on it. For both methods, a crystal containing the desired amount of ions can be produced by repeating the unit cell in x-, y- and z- direction a certain amount of times. An anhydrous LiCl crystal was made of 8x8x8 unit cells. An anhydrate unit cell contains 4 lithium plus 4 chloride ions, therefore the simulation box contained 4096 ions in total. Because the unit cell of the monohydrate contains 8 particles of each species, the monohydrous crystal was built with 8x8x4 unit cells, thus adding up to the same amount of LiCl.

An energy minimisation was carried out first. Initial velocities were assigned randomly from a Gaussian distribution with temperature 0.01 K. The equilibration run was then started. First, the temperature was ramped up to 300 K in NVT ensemble and subsequently the pressure was ramped down to 1 atm while keeping the temperature at 300 K in N σ T ensemble. Both thermostat and barostat were of the Nosé-Hoover type. After reaching the desired T and p values, the system was given 600 ps to settle, see Section 2.5 for the justification of this simulation time.

The same procedure was used for the monohydrous salt. The presence of water introduced two additional settings. During the energy minimisation, the standard SPC/E parameters K_b and K_b for bonds and angles were multiplied by 10 to make them stiff. After this, the *SHAKE* algorithm was used making these parameters redundant.

2.4.1 Surface configurations

To study the influence of irregularities in the salt surface, 4 configurations of anhydrous LiCl were simulated as shown in Figure 2.7:

- Flat no irregularities
- Ridge step in height along the x-axis
- Dent square-shaped cut-out of 1 atom thickness, 8x8 atoms
- Stub square-shaped extrusion of 1 atom thickness, 8x8 atoms

The reasons for simulating these different crystals will be discussed in Section 3.3, for now only the setting up of the crystal configurations is explained.

After equilibrating the salt crystal in bulk as described in the previous paragraph, the length of the simulation box along the z-axis was enlarged. The crystal, 41 Å in height, now had 60 Å of vacuum above and below it. This is shown in Figures 2.8 and 2.9. All boundary conditions were kept periodic for the PPPM to work. Therefore there were now infinite slabs parallel to the xy-plane placed 120 Å apart along the z-axis.

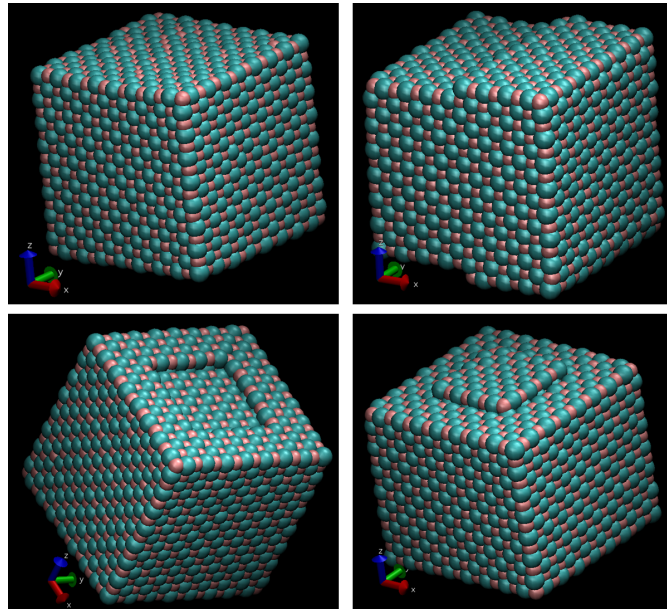


Figure 2.7: *Flat, Ridge, Dent and Stub configurations.* All boundaries are periodic, but there is empty space above and below the crystals as shown in Figure 2.9.

The Flat surface was hereby ready. For Stub, Ridge and Dent, partial layers were removed by defining the regions in which they were and using the *delete atoms* function of LAMMPS.

Finally, all crystals were equilibrated in NVT ensemble for 200 ps before water could be added.

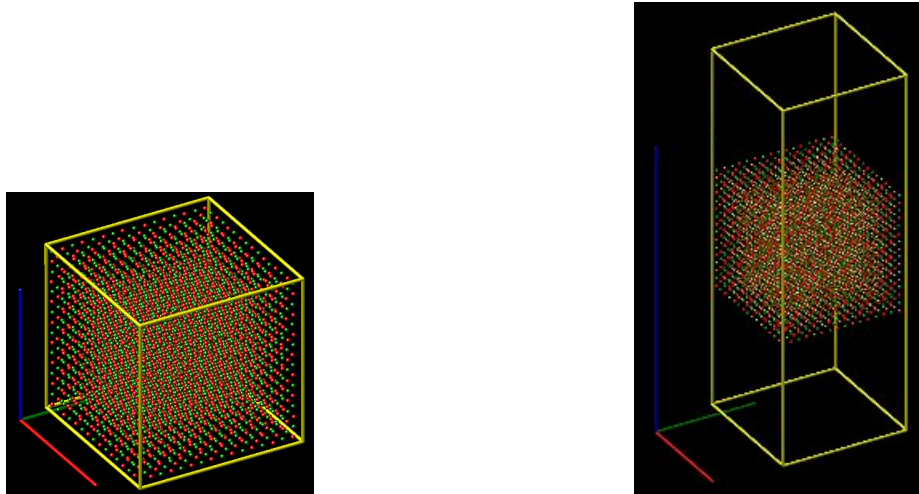


Figure 2.8: *Periodic box used to simulate LiCl bulk crystal*

Figure 2.9: *Extended box with empty spaces above and below the crystal*

2.5 Equilibration

Equilibrium is the state in which the thermodynamic potential of a system has reached a minimum. For the NVT ensemble this means that the Helmholtz free energy is at a minimum. [35] In practice however, only potential energy is measured. Therefore a system is said to be in equilibrium when its potential energy is stable.

The easiest way to check for equilibrium would be to plot the energy as a function of time and see when the energy stabilises. However, in NVT and N σ T ensembles there will always be energy fluctuations. Even in NVE ensembles simulated with MD there will still be small energy fluctuations because of errors from rounding off. Figure 2.10 shows the potential energy of the LiCl crystal containing 4096 particles during the process of ramping temperature and pressure followed by equilibration. The phases in this process were, as discussed in Section 2.4 are:

- Ramping up the temperature from 0.01 K to 300 K in NVT ensemble, duration 100 ps
- Relaxation in NVT ensemble at 300 K, duration 100 ps
- Ramping down the pressure from its current value, $4.6 \cdot 10^5$ atm, to 1.0 atm in N σ T ensemble, duration 200 ps
- Relaxation at 300 K, 1.0 atm in N σ T ensemble, duration 600 ps

The four phases can be easily distinguished in Figure 2.10. For clarity, plots of temperature and pressure are given in Figure 2.11. It can also be seen that energy fluctuations stay present and do not become smaller in time. However, there are clear plateaus. If a system has been given some time to relax after changes in e.g. temperature or pressure and such a plateau is seen in the potential energy, the system can be assumed to be in equilibrium.

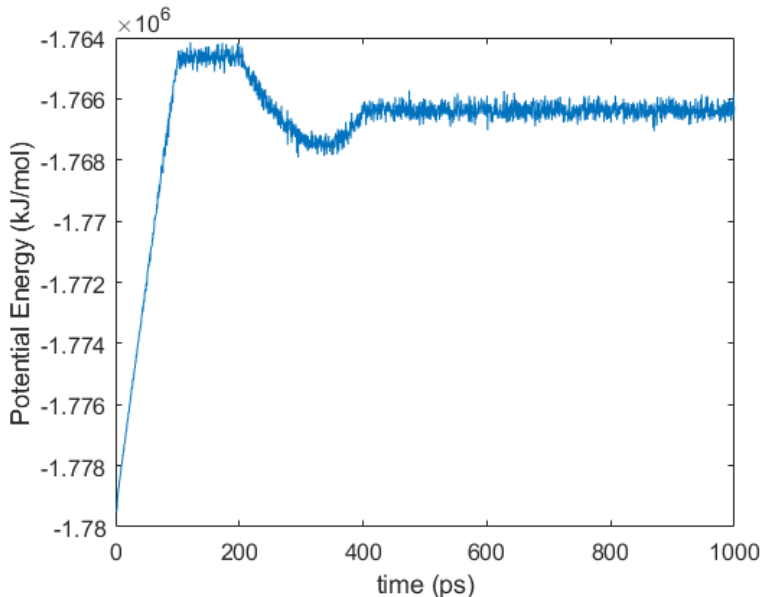


Figure 2.10: *Potential energy of anhydrous LiCl crystal in bulk during temperature and pressure ramping and relaxation*

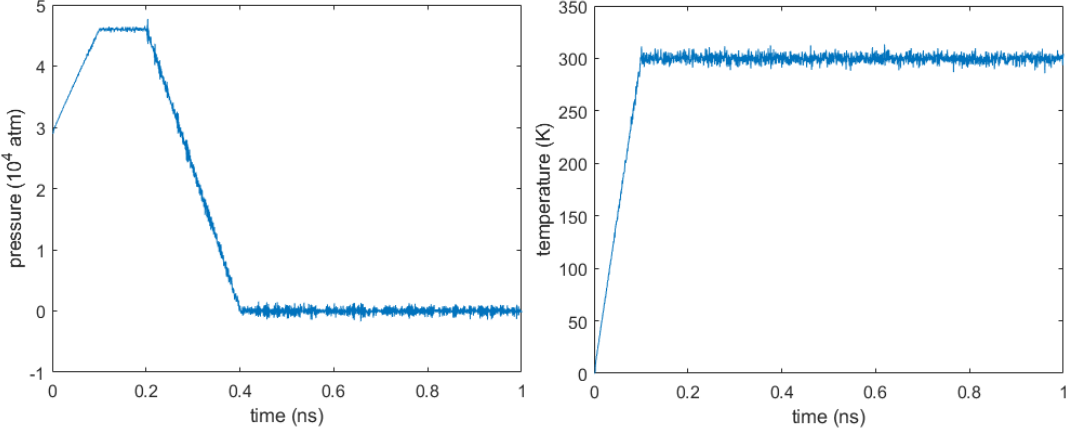


Figure 2.11: Pressure (left) and temperature (right) during ramping and relaxation

The temperature and pressure are adjusted by the thermostat and barostat throughout simulations and will always show some fluctuation around the desired values. During the last 200 ps of the run described above, the temperature fluctuated between values of 288 K and 313 K with a standard deviation of 4.2 K. The pressure fluctuated between $-1.6 \cdot 10^3$ atm and $1.7 \cdot 10^3$ atm with a standard deviation of 611 atm. Fluctuations of the cell dimensions will be discussed in Section 3.1.

Figure 2.12 shows an extra check for equilibrium, the distribution of measurements of potential energy. In equilibrium, these values are expected to have a Gaussian distribution. The histogram of the last 200 ps of aforementioned run is shown next to that of an extension of the run of 1 ns. As can be seen, both distributions are Gaussian, proving that the system was rightfully assumed to be in equilibrium.

The standard error of the measurements shown in Figure 2.12 is 10.2 kJ/mol for the 200 ps interval and 4.5 kJ/mol for the 1 ns extra run. The standard deviations are 204 kJ/mol and 202 kJ/mol, respectively, for the whole simulation box containing 2048 units of LiCl. This small difference again proves that the system can be considered to be in equilibrium during the last 200 ps of the run described above.

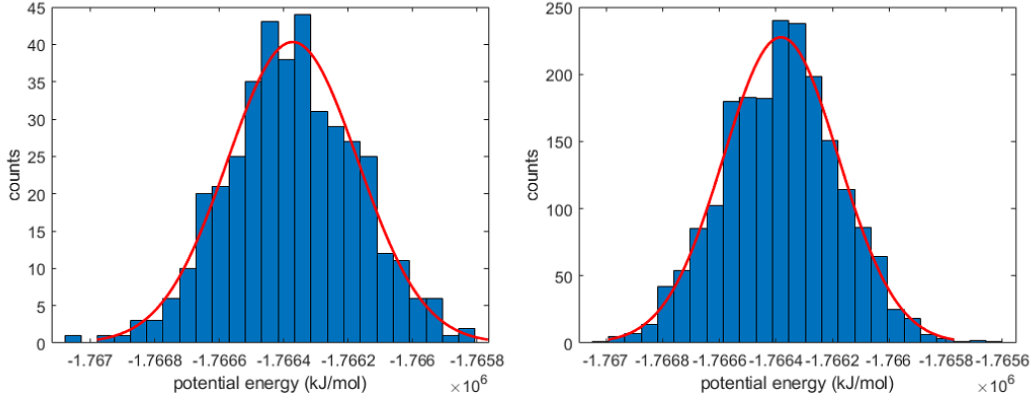


Figure 2.12: Histograms of the potential energy during the last 200 ps (left) and during a 1 ns extra run (right). Both show a Gaussian distribution, showing that the system is in equilibrium.

2.6 Water Adding

Different amounts of water molecules were added to the four salt surface configurations. First boxes with the desired amounts of water were made using the *create atoms* function. Energy minimisations were then run on these to resolve any issues of water molecules being too close to each other. These water boxes could subsequently be added to the various salt systems. The water was then given time (1 ns) to form a smooth film while keeping the salt crystal still. This was done by excluding the salt ions from integration whereby they had zero velocity and stayed at the same position. This way all water-salt simulations could be run with a smooth film and exactly the same initial configuration of the salt.

The NVT ensemble was used to simulate a crystal-water vapour interface. $N\sigma T$, besides from fluctuating a lot in box size because of large pressure fluctuations of the water, would also make the box height too small, resulting in a salt-water-salt sandwich instead of the desired salt-water-vacuum.

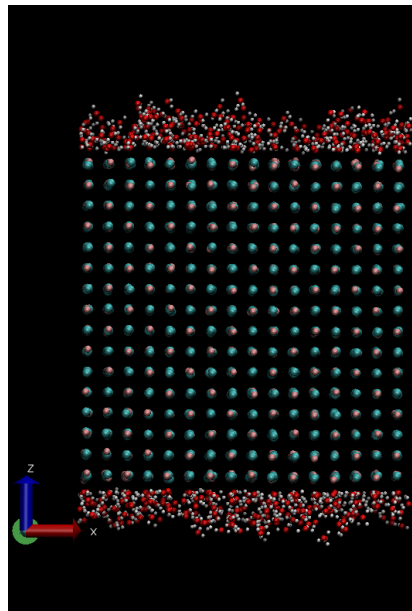


Figure 2.13: Flat crystal with water films on the surfaces

2.7 Computational Resources and Software

The MD simulations regarded in this thesis involved thousands of atoms making millions of time steps. To provide the necessary computational power, the simulations were run on the Compass cluster of the Applied Physics department of TU/e (~ 1200 Intel Xeon cores) and the national supercomputer Cartesius ($\sim 48k$ cores) of the HPC SurfSara computational center in Amsterdam.

The software used was the Large-scale Atomic/Molecular Massively Parallel Simulator (LAMMPS) by Sandia National Laboratories [20].

Chapter 3

Results & Discussion

3.1 Benchmarking

Before simulations of water and ion dynamics could be run, a choice had to be made on which force field parameters were best suited for the study at hand. As discussed in Chapter 2, the force field of lithium and chloride is defined by parameters for the Lennard-Jones and Coulombic potentials. The same holds for the water models that were regarded, supplemented by data of the bonds and angle within the water molecule. In their study, Moucka et al. [13] compared simulations in which the LJ parameters of LiCl differed per water model.

In order to decide which water model and associated force field parameters of the salt to use, the available options needed to be tested. An important first test was to see if the simulated crystals were stable; do they stay in crystalline form and is this the same form as seen in experiments? Once this test was passed, other properties of the simulated crystal were compared to their experimental values. This is called benchmarking.

The simulations were initialised with input parameters from Moucka et al. [13]. An overview of the data used is given in Section 2.3.3 and Appendix A.1. The crystals were equilibrated as described in Chapter 2. As shown in Figure 2.10, the potential energy stabilises very quickly once the temperature and pressure are at the desired values. Benchmarking data was gathered only during the last 200 ps, thus ensuring that equilibrium had been reached and no transient phenomena were taken into account.

Firstly, the stability of the anhydrous LiCl crystals was checked at room temperature and atmospheric pressure. Also, the cell dimensions of the equilibrated crystals were compared to their experimental values from the crystallographic information file. [18]

Secondly, the same was done for the monohydrous crystals. The presence of water in these monohydrates meant that also the water models needed to be implemented, including the *SHAKE* algorithm. [34] For the TIP4P-Ew the whole simulation was unstable. This turned out to be a problem in LAMMPS itself, see [36].

Thirdly, the hydration energy was calculated. From Moucka [13] it was already known that the potential energies of both the anhydrate and monohydrate cannot be expected to be very precise because the model is optimised for correct energies of solutions and not so much for the solid salt.

During simulation, the values of crystal properties were written into a logfile every 500 fs. The data of the last 200 ps of the run were then analysed further.

A full overview of the benchmarking data is given in table 3.3. Here a is the length of the simulation box along the x-axis and α is one of the three angles defining how tilted the planes of the box are, see section 2.1. SD stands for standard deviation. Since the differences in length along the x-, y- and z-axis are small, as well as the differences in angles, it is more practical to look at the a length and α angle only. The lengths are given in table 3.1.

Table 3.1: Mean of length a [\AA] of unit cells compared to their experimental values

	anhydrate		monohydrate	
	simulation	experiment	simulation	experiment
SPC/E	5.26	5.13	7.65	7.63
TIP3P	5.15	5.13	7.40	7.63
TIP4P-Ew	5.21	5.13		7.63

The TIP4P-Ew water model cannot be used because of problems with simulation in LAMMPS. The experimentally obtained unit cell length is 5.13 \AA [18] for the anhydrate. The mean value of the TIP3P simulation is closer to this value than the SPC/E simulation.

The experimentally obtained value of unit cell length along the x-axis of the monohydrate is 7.63 \AA [18]. This is very close to the number from the SPC/E simulation. The TIP3P simulation gives a slightly lower value.

For both models, the angle α is very close to the experimental value of 90 degrees, see Table 3.3.

Since this study is done in the scope of hydration of lithium chloride, it is good to know if the change in enthalpy, $H = E + pV$, corresponds to its experimental value. Here E [J] is the internal energy, composed of potential and kinetic energy, p [Pa] the pressure and V [m^3] the volume.

From Donkers [4], the hydration enthalpy ΔH from anhydrous to monohydrous LiCl is known to be 62.9 kJ/mol. Pressure is a highly fluctuating quantity in MD simulations. Because the value of mechanical work is small compared to the internal energy anyway, this term was left out of consideration. The kinetic energy is directly related to temperature, which is continuously corrected by the Nosé-Hoover thermostat. We therefore only consider the potential energy. The difference in potential energy between the anhydrate and monohydrate is compared to the experimental hydration enthalpy. Both are lower than the value from experiment, see table 3.2. This was expected, as stated above, but SPC/E is much closer.

Table 3.2: Potential energy per mole of LiCl [kJ/mol] and the difference between anhydrate and monohydrate compared to the experimental value of hydration enthalpy [kJ/mol]

	anhydrate	monohydrate	difference	experiment
SPC/E	-862.5	-913.7	51.2	62.9
TIP3P	-882.3	-923.8	41.5	62.9
TIP4P-Ew	-868.5			62.9

Moucka showed that only the SPC/E model gives a solubility close to the experimental value. Benchmarking showed that both SPC/E and TIP3P simulations gave good results regarding crystal dimensions. SPC/E had better agreement in hydration energy. Altogether, this makes SPC/E the best option to work further with.

Table 3.3: Top to bottom: lengths (Å), angles (degrees) and potential energies (kJ/mol) of anhydrate (top 3) and monohydrate (bottom 3). SD stands for standard deviation.

	mean	SD	minimum	maximum					
	a	b	c	a	b	c	a	b	c
SPC/E	5.26	5.26	5.6 · 10 ⁻³	5.1 · 10 ⁻³	5.3 · 10 ⁻³	5.24	5.25	5.25	5.28
TIP3P	5.15	5.15	6.9 · 10 ⁻³	6.8 · 10 ⁻³	6.5 · 10 ⁻³	5.13	5.13	5.13	5.17
TIP4P-Ew	5.21	5.21	6.9 · 10 ⁻³	6.9 · 10 ⁻³	6.6 · 10 ⁻³	5.19	5.19	5.19	5.23

	mean	SD	minimum	maximum					
	α	β	γ	α	β	γ	α	β	γ
SPC/E	90.0	90.0	90.0	0.05	0.06	0.08	89.8	89.8	90.1
TIP3P	90.0	90.0	90.0	0.06	0.07	0.07	89.8	89.8	90.2
TIP4P-Ew	90.0	90.0	90.0	0.07	0.07	0.06	89.8	89.8	90.2

	mean	SD	minimum	maximum					
	α	β	γ	α	β	γ	α	β	γ
SPC/E	-862.5	0.099	-862.8	-862.2					
TIP3P	-882.3	0.096	-882.6	-882.1					
TIP4P-Ew	-868.5	0.103	-868.9	-868.3					

	mean	SD	minimum	maximum					
	α	β	γ	α	β	γ	α	β	γ
SPC/E	7.65	7.92	7.78	6.6 · 10 ⁻³	7.4 · 10 ⁻³	6.9 · 10 ⁻³	7.63	7.90	7.76
TIP3P	7.40	8.05	7.65	5.4 · 10 ⁻³	9.4 · 10 ⁻³	6.7 · 10 ⁻³	7.39	8.02	7.63
TIP4P-Ew	90.0	90.0	90.0	0.06	0.08	0.11	89.8	89.8	90.2

	mean	SD	minimum	maximum					
	α	β	γ	α	β	γ	α	β	γ
SPC/E	90.0	90.0	90.0	0.07	0.06	0.08	89.8	89.8	90.2
TIP3P	90.0	90.0	90.0	0.06	0.08	0.11	89.8	89.8	90.3

	mean	SD	minimum	maximum		
	α	β	γ	α	β	γ
SPC/E	-913.7	0.147	-914.1	-913.2		
TIP3P	-923.8	0.155	-924.2	-923.4		

3.2 Water Structure and Dynamics at a Flat Surface

Simulations were run of water films with varying amounts of water on "flat" salt surfaces, i.e. salt crystals that had no ions removed from their top and bottom layers. Runs of up to 50 ns with up to 512 water molecules per film (one above and one below the crystal) were done and none resulted in any ions dissolving. The amount of 512 water molecules per film corresponds to 4 water molecules per lithium ion at the surface. The result agrees with the MD study of Bahadur et al. [9] in which NaCl crystals with no lattice defects did not dissolve at all. Therefore, at flat surfaces only the behaviour of water near the salt crystal was looked into. Specifically, self-diffusion of the water and orientation of water molecules.

3.2.1 Translational self-diffusion of water

The translational diffusion of water was studied first. Initially it was calculated from Mean Square Displacement (MSD) output from LAMMPS. The *MSD* function sets initial positions $\vec{r}_i(0)$ for all particles at the moment the function is first called. After this, displacements are calculated with respect to these initial positions. The x-component of MSD is defined as

$$\overline{(x(t) - x(0))^2} = \frac{1}{N} \sum_{i=1}^N (x_i(t) - x_i(0))^2, \quad (3.1)$$

with N the amount of particles considered.

Figure 3.1 shows a plot of MSD data from LAMMPS of films containing 128 water molecules per film, corresponding to 1 water molecule per lithium ion at the surface. Steps in displacement in the z-direction are visible. These were visually confirmed in VMD [8] to be caused by single water molecules evaporating and migrating from the top water layer to the bottom or vice versa. This also explains the jump in the x- and y-component, evaporated water molecules can move freely in vacuum. To calculate diffusion within the water films, only data between these migration instances could be used.

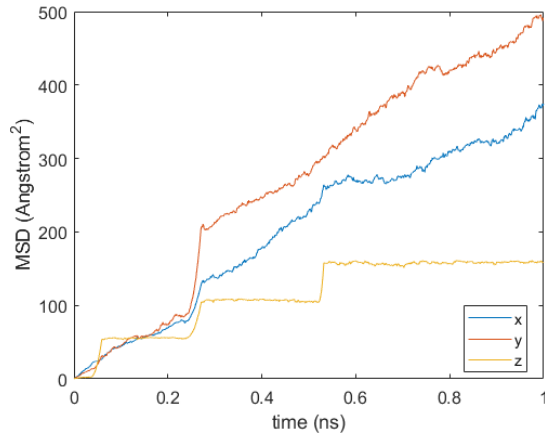


Figure 3.1: *MSD of 2x128 water molecules showing step behaviour in the z-component. Obtained with the MSD function in LAMMPS.*

The x-, y- and z-components of diffusion were calculated for water films containing various amounts of water molecules. This was done using the Einstein relation,

$$2D\Delta t = \overline{(x(t) - x(0))^2}, \quad (3.2)$$

analogous for the y- and z-component.

Besides the problem of migrating molecules, the single initial positions $\vec{r}_i(0)$ LAMMPS uses give no opportunity for improving statistics. Figure 3.2 shows diffusion coefficients of different amounts of water calculated from the LAMMPS MSD data. Two problems are visible.

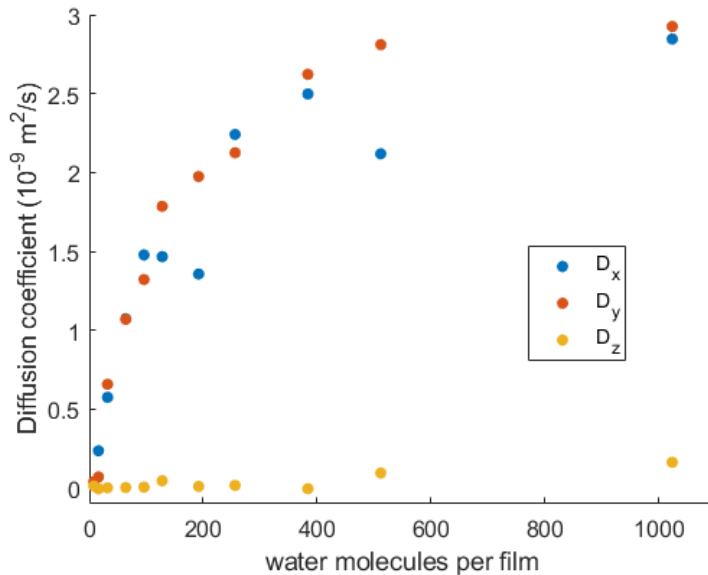


Figure 3.2: *Diffusion of increasing amounts of water using MSD data from LAMMPS. The values of D_x and D_y are unexpectedly far apart for films of 128, 192 and 512 water molecules. The crystal surfaces (top and bottom) contained 128 lithium and 128 chloride ions per surface. D_z stays very low and is sometimes even negative, showing that use of LAMMPS MSD data does not give reliable diffusion coefficients.*

Firstly, the values of D_x and D_y are sometimes quite widely apart. This should not be the case since everything is symmetric in the xy-plane.

Secondly, D_z stays very low and is even sometimes negative. For large amounts of water this is unexpected because the water film becomes thicker for larger water counts, making more free movement possible. For example, if $D = 2.25 \cdot 10^{-9} \text{ m}^2/\text{s}$ this means that in 0.5 ns a water molecule will on average have moved $1.5 \text{ nm} = 15 \text{ \AA}$. This is roughly the thickness of a film with 512 water molecules as can be seen in Figure 3.3. Even in the thickest films of 1024 water molecules, D_z is far lower than expected.

Diffusion was therefore further looked into by using a self-made script. This made it possible to ignore the migrating water molecules, average over multiple time intervals and hereby also calculate diffusion coefficients with various (small) interval lengths. Now $\vec{r}_i(0)$ was set at the start of each time interval instead of just once. Results are shown in Figure 3.4. The length of time-intervals used in these measurements was 100 ps. The simulation time was 1 ns, so values of diffusion coefficients were averaged over 9 measurements. D_x and D_y values are now closer together and D_z increases with the water count, nevertheless, remaining smaller. Given that the thickness of the water films is difficult to define, D_z agrees with expectation.

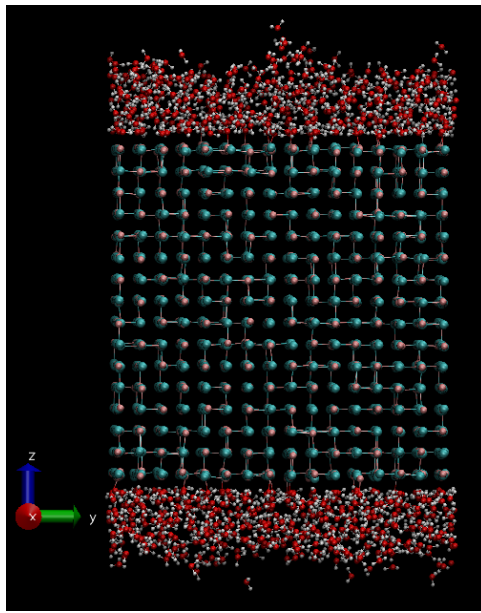


Figure 3.3: Films containing 512 water molecules above and below the LiCl crystal. Height of the crystal is 40 Å.

The increase of the x- and y-components of diffusion with increasing water counts suggests that proximity to the salt slows down movement of the water. This effect is strong for low water counts because here all water is close to the salt and there is no shielding by closer layers.

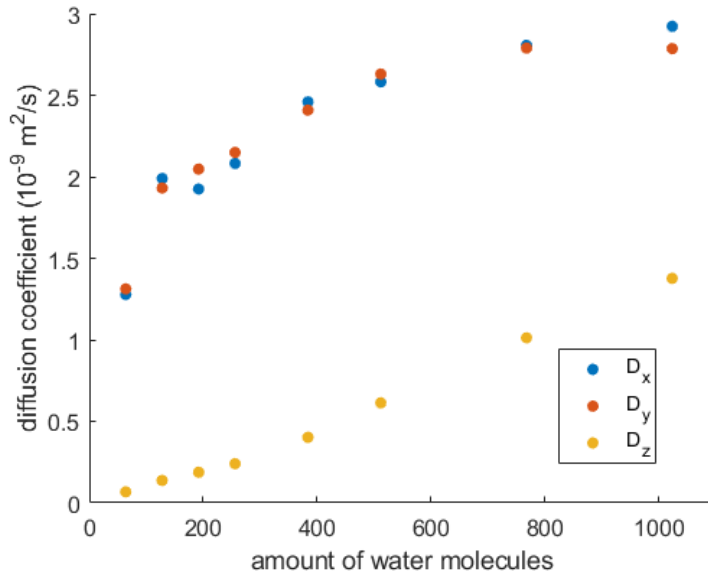


Figure 3.4: Diffusion of increasing amounts of water using own script, with 100 ps intervals. The total simulation time was 1 ns, so averages were obtained over 9 values. Now results are as expected. For reference, D of pure water in bulk using these force fields is roughly $3 \cdot 10^{-9} \text{ m}^2/\text{s}$.

The diffusion coefficient was also calculated with various time-intervals between measurements. The case of 1024 water molecules per film is shown in Figure 3.5. Since the films have only a small thickness, the possibility of movement in the z-direction is limited. For long values of Δt , this has a big effect on the calculated D_z . For $\Delta t < 100$ ps also the x- and y- diffusion increases. Since it is the long-range diffusion we are interested in and not short-range movements within clusters, the value of $\Delta t = 100$ ps was chosen for further calculations.

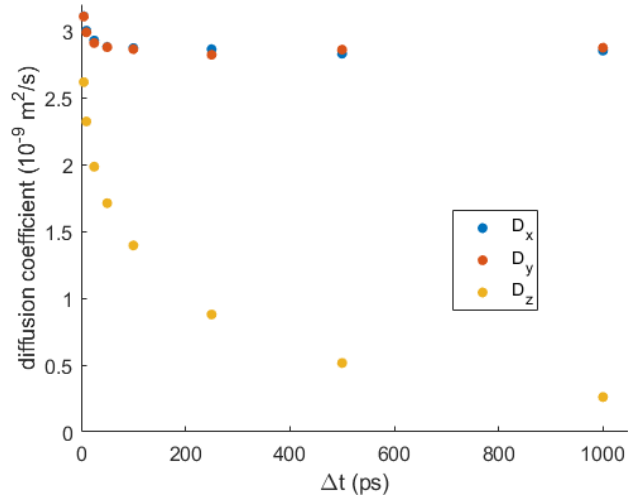


Figure 3.5: *Diffusion of 1024 water molecules per film as a function of time-interval length. Longer time intervals result in lower values of D_z because movement in the Z-direction is limited by the film thickness. At short time-intervals $\Delta t < 100$ also D_x and D_y increase because short-range interactions within water clusters become prominent. Total simulation time was 10 ns.*

3.2.2 Orientation of water molecules

From literature it is known that water molecules have a preferred orientation with respect to the salt surface. Firstly, this was looked into as a function of the amount of water per film. Secondly, the density profile of the water films was measured. Finally, the profile measurements were used to study the orientation at a certain distance from the salt.

Figure 3.6 shows the orientations of water molecules surrounding a lithium and chloride ion. Because of their electrical charges, lithium ions attract oxygen atoms while repulsing hydrogen atoms while for chloride ions it is the other way around. The Coulombic interaction together with the Lennard-Jones potential determine how close water molecules will approach the respective ion species.

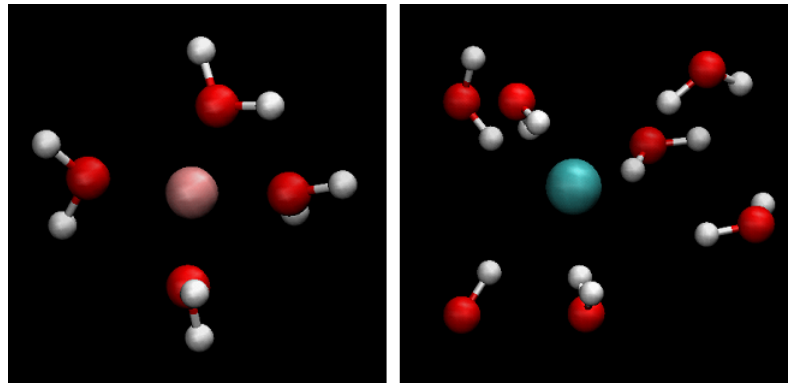


Figure 3.6: Water molecules near lithium (left) and chloride (right) ions show a distinct orientation. Pictures were made with VMD, showing dissolved ions in a Stub system with 1024 water molecules per film.

Lithium and chloride ions have different radii. This is expressed in their σ values for the Lennard-Jones potential of 1.4 Å and 4.8 Å respectively. For the LJ potential of interaction with oxygen, the Lorentz rule gives 2.3 Å for O-Li and 4.0 Å for O-Cl. Since hydrogen plays no role in the LJ potential, water can be closer to lithium than to chloride. Furthermore, since an oxygen atom within water has a negative electrical charge, it will be drawn towards positively charged lithium. Because of this, we expect preferential water orientation near the salt surface, which was studied first.

Figure 3.7 shows the interaction energy of a single water molecule with a single ion. The minima in potential energy are at roughly at 3 Å for chloride and 2 Å for lithium, closer than the σ values because of attractive Coulombic forces. Since the potential energy is lower when a water molecule is close to a lithium ion, it is expected that most waters near the salt surface will be close to lithium ions and pointed towards the crystal surface. An example of a water molecule close to the salt surface is shown in Figure 3.8.

Orientation of water molecules was defined as the angle of their dipolar moment with the z-vector. This way, a preferable orientation will be visible as mirrored images for top and bottom water films. Angles were measured every ps of a 1 ns simulation and the total counts were plotted in histograms.

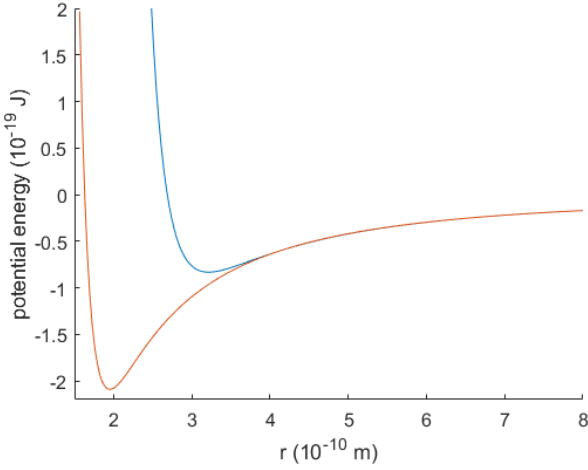


Figure 3.7: Potential energy of one water molecule near one Cl ion (blue) or one Li ion (red). Because the lithium ion is smaller, water can approach closer and the minimum in potential energy is lower than for chloride.

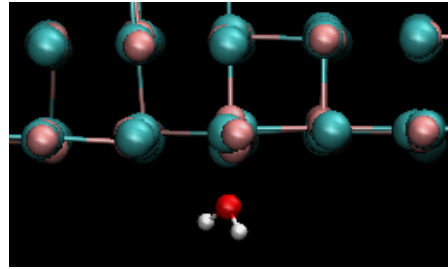


Figure 3.8: Snapshot of a water molecule close to the salt surface. The angle of this molecule to the z-vector is roughly 180 degrees.

There are 128 lithium ions in the top layer, as well as in the bottom layer. This means that for films of 64 water molecules, there are 2 lithium ions available per water molecule and the expected orientation should be visible. Figure 3.9 indeed shows a clear difference between water films on top of and below the salt. More angles lower than 90° are seen in the top film while in the bottom film most angles are higher than 90°. The mean values are 70° for the top film and 110° for the bottom film. The difference in total amount of molecules per layer is caused by evaporation and migration, the films do not contain exactly 64 water molecules all the time.

For the higher amount of 512 molecules per layer there is still a visible difference between the films, but no longer a strong preference for angles above or below 90°, as can be seen in Figure 3.10. Indeed, the mean values are now 90° for both films.

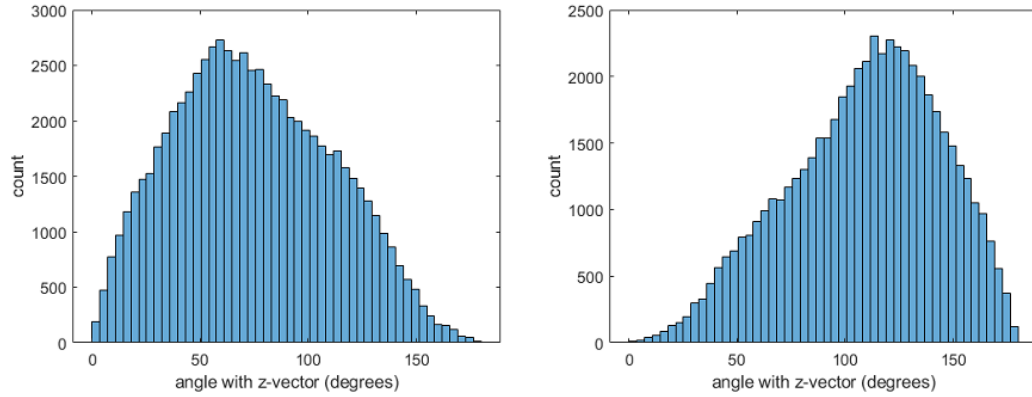


Figure 3.9: Orientations of 64 water molecules above (left) and below the salt crystal (right). Most molecules are pointed (slightly) towards the crystal. Measurements were done every ps for 1 ns.

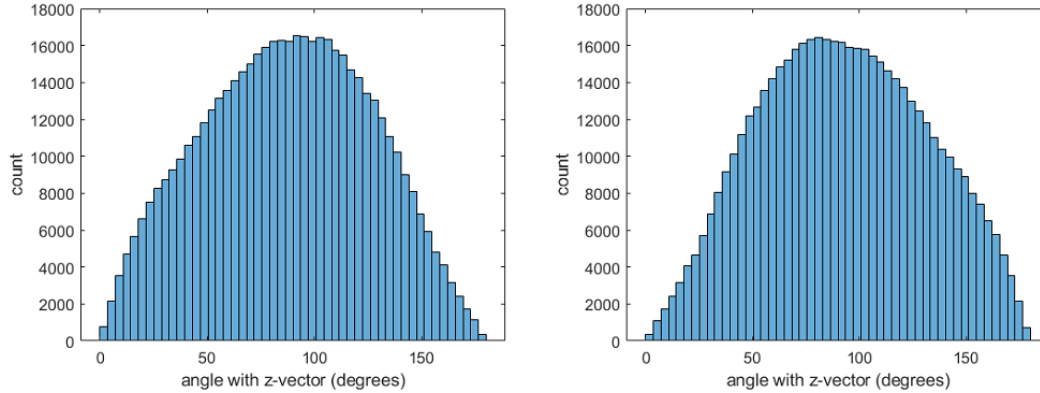


Figure 3.10: Orientations of 512 water molecules above (left) and below the salt crystal (right). There is still mirroring between top and bottom films, but no preferred orientation. Measurements were done every ps for 1 ns.

Next, density profiles of the water films were looked into. These were calculated by dividing the space above and below the crystal into slabs parallel to the XY-plane. Every 10 ps, the amount of water molecules per slab was counted by looking at the Z-coordinate of oxygen atoms. The counts per slab were then summed over a run of 1 ns.

As can be seen in Figure 3.11, there is a clear peak close to the salt surface followed by a less pronounced secondary peak. The Li-O distance from the crystal surface to the primary peak is 1.9 Å and approximately 3 Å to the second peak.

Du and Miller [16] showed that water molecules have a distinct orientation at the salt surface. In Figure 3.12 the orientations of the water molecules in the first peak are shown. Although not all angles are below 90° for the bottom film and above 90° for the top film, most molecules are pointed towards the crystal surface.

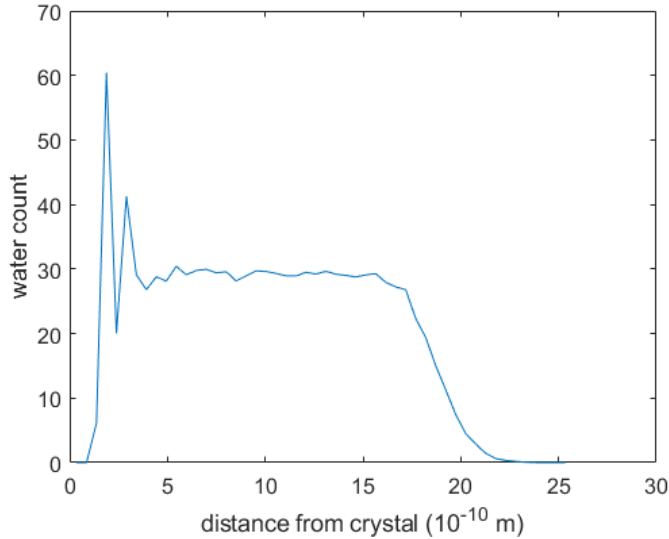


Figure 3.11: *Density profile of the top water film, containing 1024 water molecules. A pronounced peak is present at 1.9 Å from the crystal surface. Average values were obtained over 99 measurements, 10 ps apart.*

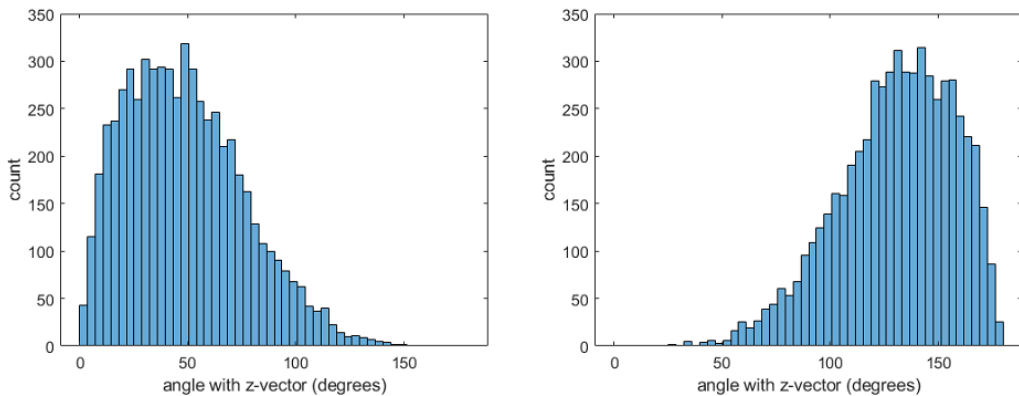


Figure 3.12: *Orientation of water molecules in the first peak, top (left) bottom (right). There is a clear preference for orientation towards the crystal. Measurements were done every 10 ps for 1 ns.*

Liu et al. [10] found layers with different orientations. They used *ab initio* molecular-dynamics simulations, however, and already state that this gives different results than classical MD. Apart from the first and second peak, no slabs were found in which the water molecules showed distinctively preferred orientations. Figure 3.13 shows the angles with the z-vector of water molecules in the second peak. Although less pronounced, a preference for an orientation away from the crystal is now visible.

Shinto et al. [37] saw different diffusions in different layers. An attempt was made to analyse water diffusion per bin. For the water molecules present in the first peak of the density profile, the diffusion values were roughly the same as in Figure 3.4 at 64 waters. The low water count makes it hard to make meaningful conclusions however. This subject was therefore, and in sake of time, not looked further into.

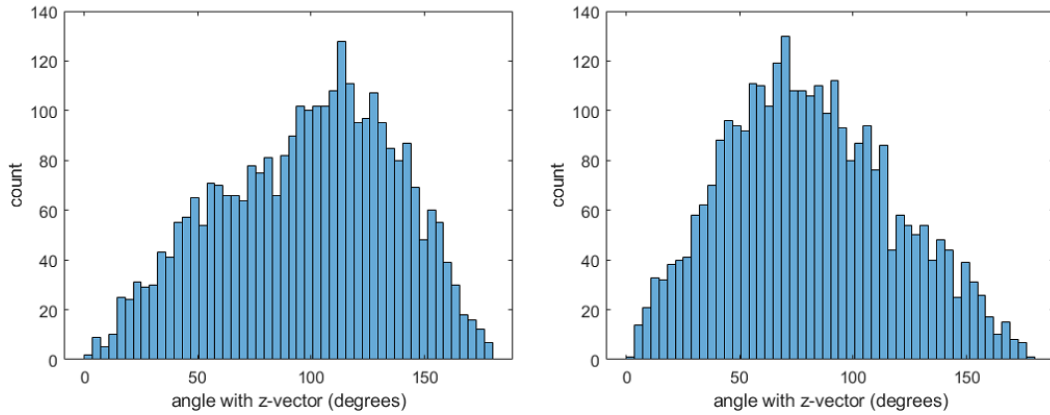


Figure 3.13: Orientation of water molecules in the second peak, top (left) bottom (right). There is a preference for orientation away from the crystal. Measurements were done every 10 ps for 1 ns.

From the observations made, we can draw two conclusions. First, when a film contains few water molecules, these mostly have their oxygen atoms closest to the crystal surface. Second, in films containing higher amounts of water, a layer of water molecules is formed at a Li-O distance of 1.9 Å from the crystal surface. These water molecules have a very strong preferential orientation towards the salt crystal. A less pronounced secondary water layer at 3 Å is formed in which the hydrogen atoms are closest to the salt crystal.

Preferential orientation was thus most strongly proved for the water molecules in the primary density peak.

3.3 Dissolution at Surfaces of Different Geometry

As discussed in the previous section, no dissolution takes place within 50 ns from a Flat crystal. Because of this, to study the dissolution of lithium chloride, defects had to be introduced to the crystal. Experimental studies, such as [38] show that "atomic steps" naturally occur on the surface of rocksalt (NaCl), which is similar to LiCl. From Lanaro and Patey [39] it is known that cubic nanocrystals dissolve faster than differently shaped ones. Therefore three types of non-flat surfaces were studied. As described in Chapter 2, these are Dent, Stub and Ridge.

The dissolution process was investigated in four ways. First, the dissolution rate as a function of water amount was studied. Second, the order in which ions go into the solvent was visualised. Third, the amount of water molecules surrounding dissolved ions was counted. Fourth, the diffusion of the solution was compared to diffusion in pure water films. These subjects are discussed in the following sections.

3.3.1 Dissolution rate for increasing water counts

Dissolution rate was studied in two ways. First, dissolution at different surface geometries was looked into. This was inspired by the study of Lanaro and Patey [39], who showed that the dissolution rate depends on the shape of nanocrystals. Second, the influence the amount of water molecules in the films has on the dissolution rate was viewed.

After equilibrating the salt crystals and subsequently the water films on them, runs were made

of increasing length. Ions were defined as dissolved if they had moved 2 Å or more from their original position in the crystal. Figure 3.14 shows the amount of dissolved ions over time for the three non-flat surfaces. For all three, the water films contained 1024 molecules per film. Three observations can be made.

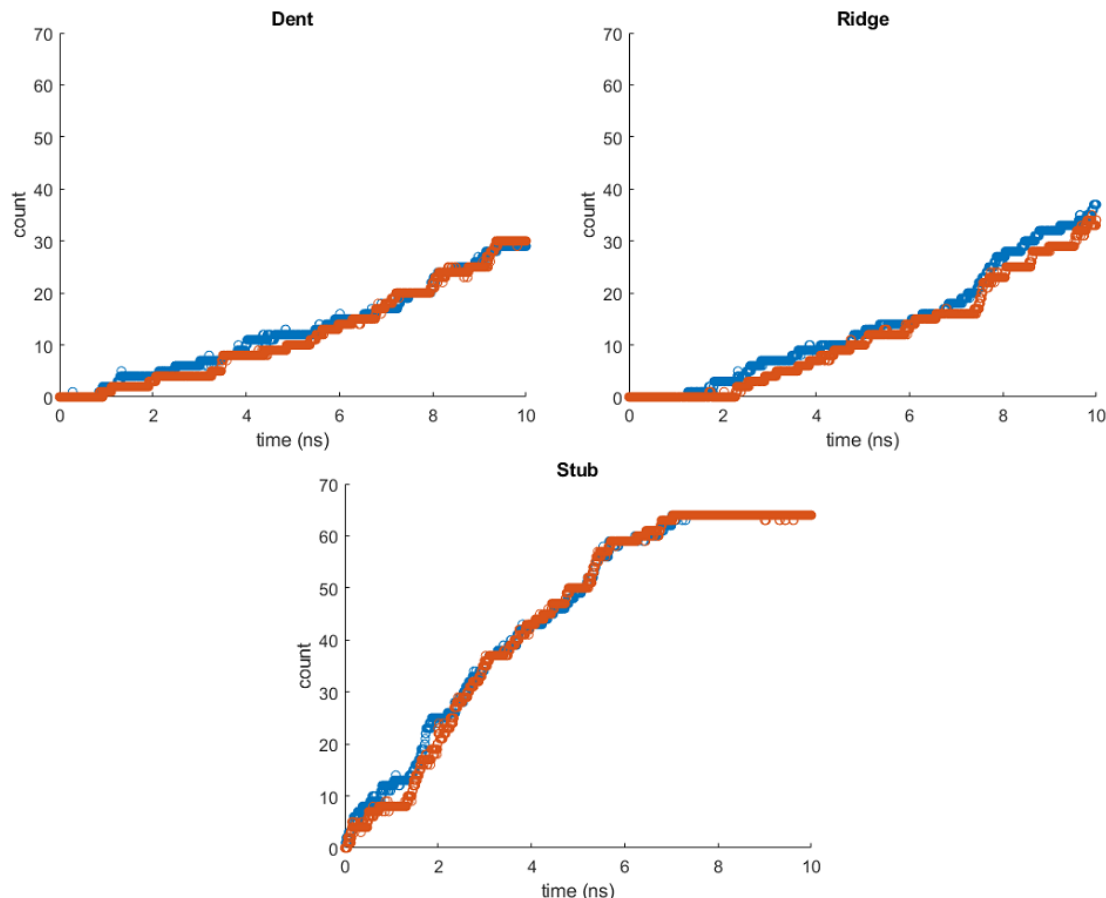


Figure 3.14: *Dissolved ion counts for Dent, Ridge and Stub. Chloride in blue, lithium in red. Water films contain 1024 water molecules.*

Firstly, in the Stub simulation all 64 ions of the top layer are dissolved within 10 ns. For Dent and Ridge, the amount of ions in solution after 10 ns are lower, lowest for Dent.

Secondly, the ion count of chloride is frequently higher than the count of lithium. This suggests that Cl leaves the crystal structure more easily. There is no clear difference in dissolution rate, neither are the counts ever wide apart for long times.

Thirdly, the lines are quite noisy. Fitting attempts gave no conclusive results. Therefore dissolution rates per se were unsuited to research further.

Instead of rates, the times at which the first and last ions of each species went into dissolution were analysed. The first and last ions were counted as dissolved when they were in solution for longer than 10 ps. Since only the Stub dissolved fully within 10 ns, this system was used to study dissolution times.

Figure 3.15 shows averaged times at which the first ion from a Stub went into solution as a function of the amount of water per film. Initial analysis of the first dissolution events gave no clear result. Five more simulations were therefore run. The water films were randomised by shortly heating up the water to different temperatures and then cooling them down back to 300K before equilibration. The averages of these 6 runs were plotted. A clear positive effect of the amount of water on the dissolution of the first chloride ion is visible. For lithium, no such conclusion can be drawn.

Figure 3.16 shows the times after which the last ions dissolve. Since simulating these full dissolutions costs large amounts of computational time, only a single run was done. For both lithium and chloride, these times seem to be lower for higher water counts.

Above 512 water molecules per film the times do not change much anymore, but more study is needed to draw wider conclusions.

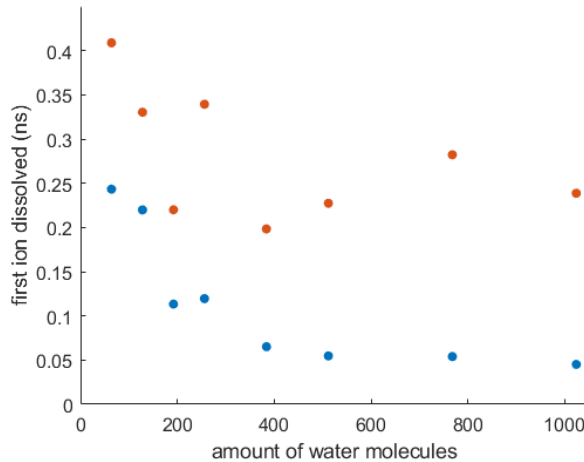


Figure 3.15: *Times of first ion in solution, averaged over 6 runs. Cl blue, Li red*

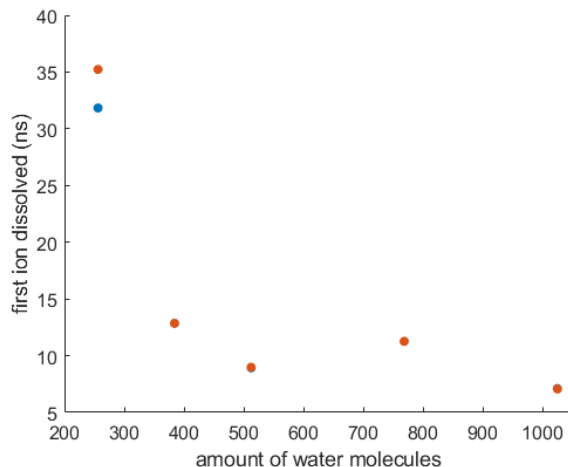


Figure 3.16: *Times of last ion in solution, single run. Cl blue, Li red. For the amounts of water >256 the red dots are on top of the blue ones i.e. the times are the same.*

3.3.2 Order of ions dissolving

Some information on the order in which lithium and chloride ions dissolve was already obtained from the dissolution rates. To gain further insight into the dissolution process, more details were wanted. Yang et al. [40] found that sodium and chloride ions from rock salt dissolve alternatingly. In contradiction, Du and Miller[16] reported a preference for lithium to dissolve, resulting in a charged LiCl salt surface. For NaCl, KCl and RbCl they found a preference for chloride to dissolve.

Figure 3.17 shows the dissolution process of a Stub. For clarity only the non-dissolved ions of the top layer are shown. The first ion to dissolve is a chloride ion on a corner. The top-left lithium ion remains near its original position quite long before dissolving. Later, also the other corner ions leave the surface. A preference for ions on corners to dissolve was expected since these ions are more accessible for water. Also, on a corner there are less directly neighbouring ions of opposite charge that prevent an ion from moving freely. In the picture in the bottom middle, a chloride ion not on a corner is dissolved. There are only lithium ions on the corners here, showing that chloride dissolves much easier than lithium.

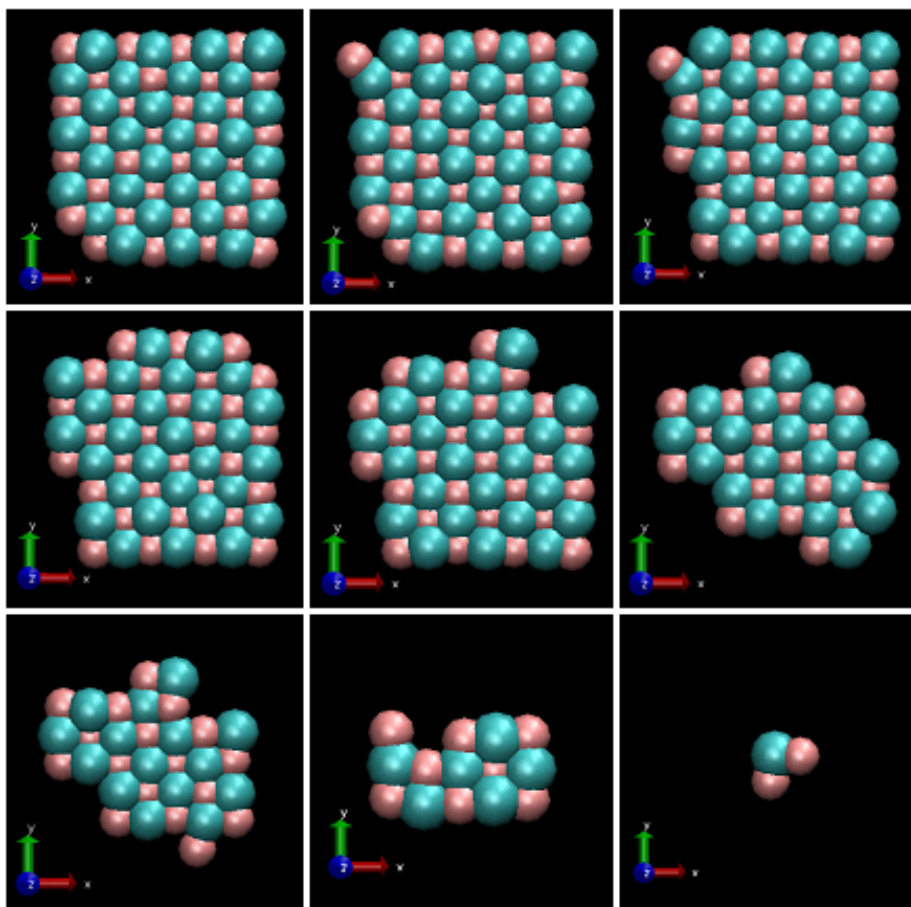


Figure 3.17: *Dissolution process of a stub, time increasing left to right and top to bottom, $t = 36, 62, 129, 279, 1072, 2472, 2911, 5439, 7005$ ps. Cl blue, Li red. Films contain 1024 water molecules. Chloride dissolves easier than lithium. Dissolution usually starts at corners.*

The dissolving top layer of a Dent system is shown in Figure 3.18. Again, chloride ions are seen to leave the crystal first. Furthermore, these first ions are close to the inner corners.

The last system, Ridge, is shown in Figure 3.19. In the right most picture, because of periodic boundary conditions, the top right chloride and bottom right lithium ion are next to each other. The same observation is made as with Dent, a new row starts to dissolve near an inner corner. This occurs before the previous row has fully dissolved.

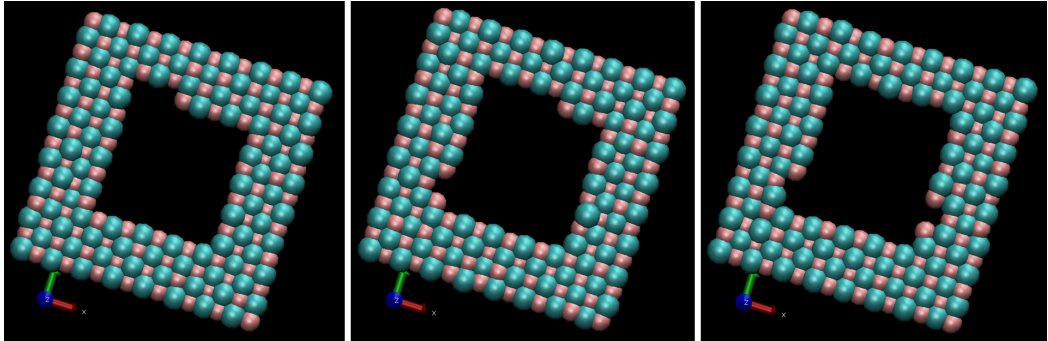


Figure 3.18: *Dissolution process of a dent, Cl blue, Li red. Dissolution of a new row starts with a chloride ion near a corner.*

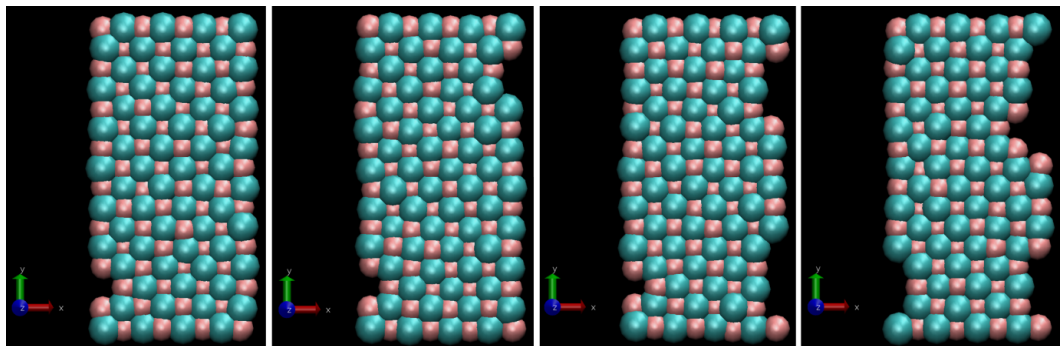


Figure 3.19: *Dissolution process of a ridge, Cl blue, Li red. Multiple holes are made in the rightmost row and a new row starts dissolving before the previous row is fully dissolved.*

In their 2011 article Liu et al. [41] state that polarisability of the Cl^- ion is the cause of preferential chloride dissolution. The force fields which were used in the simulations shown above are however non-polarisable. Oyen and Hentschke [42] used the SPC/E-P water model, a polarisable version of SPC/E, and saw adsorption of ions from solution onto a sodium chloride crystal. Recrystallisation was not observed in this study, dissolved ions stayed in solution for the duration of the simulations.

Fukushima et al. [15] describe how the alignment of water molecules near chloride ions to form a linear Cl^- -H-O bond plays a role in the preferential dissolution of chloride. They used a different potential however and similar observations were not made in our simulations. Garcia-Manyes et al. [43] used Lennard-Jones combined with Coulombic potentials and the SPC water model. They observed water molecules being more stably and closely positioned next to lithium ions than next to chloride. The higher mobility of water near chloride is, according to them, the cause of chloride dissolving more easily. This is in agreement with the conclusions from Section 3.2.2.

3.3.3 Hydration Shells

While in solution, ions are continuously surrounded by water molecules as already shown in Figure 3.6. To learn more about how the number of water molecules surrounding ions is influenced by the total amount of water in the film, measurements were made.

Jungwirth [44] calculated that six water molecules are needed to dissolve a NaCl molecule. While the minimum amount of water to dissolve ions will not change, it could be that the amount of water molecules neighbouring ions in the solution fluctuates. The neighbour count as a function of total water count per film was therefore analysed.

Water molecules were defined as neighbour if they were within a certain distance from the ion in consideration, so inside a sphere of radius r with the ion in the centre. An often used value of r is the Lennard-Jones parameter σ . However, vibrations made counts fluctuate heavily while for a larger r the water molecules maintained their orientation relative to the ion as checked with VMD. Therefore, for lithium the radius was set to 3 Å and for chloride to 4 Å. Measurements were made on Stub systems in which all ions of the extrusions had been dissolved. Neighbour counts per species were averaged over all dissolved ions in both films, 64 chloride and 64 lithium ions.

In Figure 3.20 the average neighbour counts in four films are shown. The values of the 512 and 768 films are the same, 4 neighbours for lithium and 7 for chloride. In the 256 and 384 films lower counts are seen however, lowest in the 256 film. We can therefore conclude that there is indeed an influence of the total amount of water per film on the neighbour count.

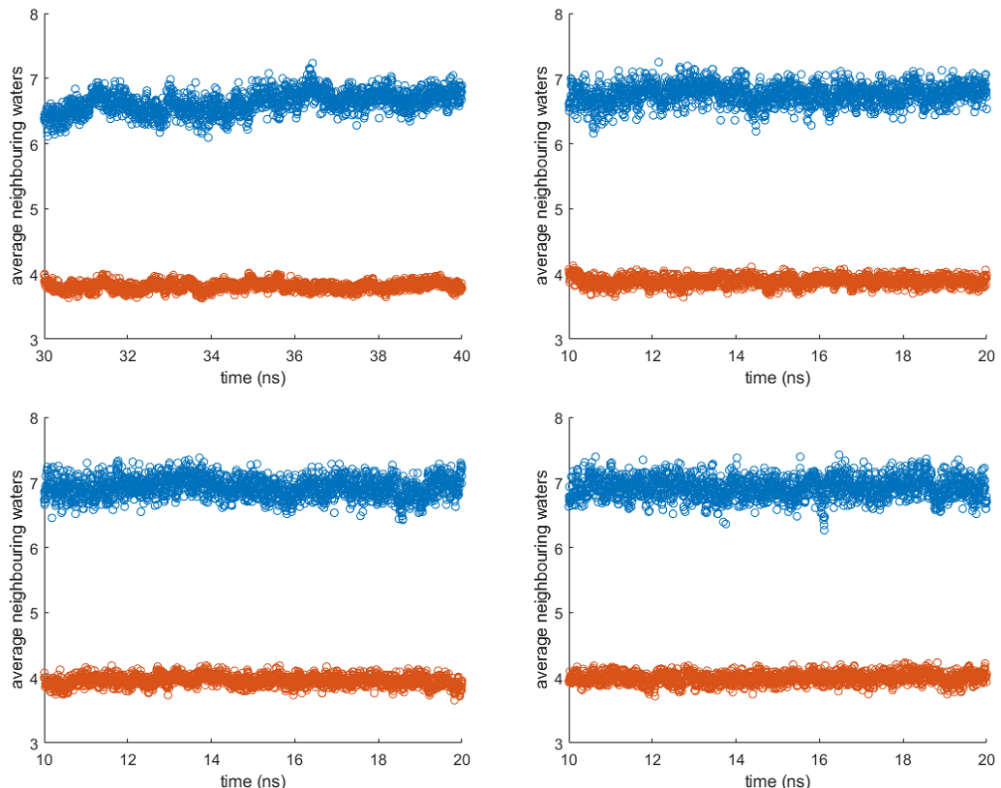


Figure 3.20: Average neighbour counts for films of 256 (top left), 384 (top right), 512 (bottom left) and 768 (bottom right) water molecules per film in which all extruding ions of a Stub had been dissolved. In the 512 and 768 films, chloride ions have 7 neighbouring water molecules and lithium ions have 4. The 384 and 256 films show lower values, lowest for the 256 film.

3.3.4 Mobility of Water and Ions in Solution

The mobility in films of solution was studied. First, the diffusion of water in solution was investigated. Second, the diffusion of the dissolved ions was analysed.

The self-diffusion of water in films of solution was compared to its value for films containing no salt ions. This was done by analysing solutions in which all 32 lithium and 32 chloride ions per extrusion of a Stub had been dissolved. Hereby the salt surfaces had become flat and therefore the measurements are directly comparable to those of the Flat simulations in Section 3.2.1.

Diffusion coefficients were calculated from MSD values using 100 ps intervals, as described in Section 3.2.1. Simulations of 10 ns were used, giving 99 time-intervals to average over.

Figure 3.21 shows the self-diffusion of water in the solution containing 128 ions and of pure water films. As in pure water films, the diffusion increases with increasing amounts of water molecules in the films. The values are significantly lower than for pure water, showing that water molecules are limited in their motion by the presence of dissolved ions.

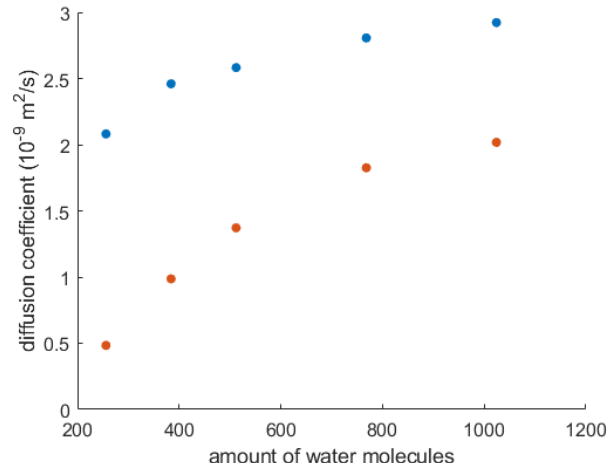


Figure 3.21: *Diffusion coefficient D_x for various amounts of water molecules per film of solution (red) and pure water (blue). Interval length was 100 ps, averages were taken over 99 measurements. For reference, D of pure water in bulk using these force fields is roughly $3 \cdot 10^{-9} \text{ m}^2/\text{s}$.*

McCall and Douglas [45] found a linear relation between ion concentration and the self-diffusion of water in these solutions. Figure 3.22 shows the ratio of diffusivity in solutions and diffusivity in pure water films. Here the diffusion coefficients in the xy-plane were used, $D = \frac{D_x + D_y}{2}$ and the same was done for the pure water values D_0 . Concentration was defined here as $\frac{\text{total number of ions}}{\text{total number of water molecules}}$. Both measurements from simulations and the values from McCall and Douglas are plotted.

Indeed, we see a linear dependency of diffusion on concentration. The lowest diffusion coefficients deviate from the linear trend, both the values from simulation and from literature. There is a difference in slope of the literature and simulation values. The measurements by McCall and Douglas were made in bulk. A possible cause for the difference in slope is thus the presence of the LiCl crystal in the simulations. Also, the force fields used could have an influence on diffusion.

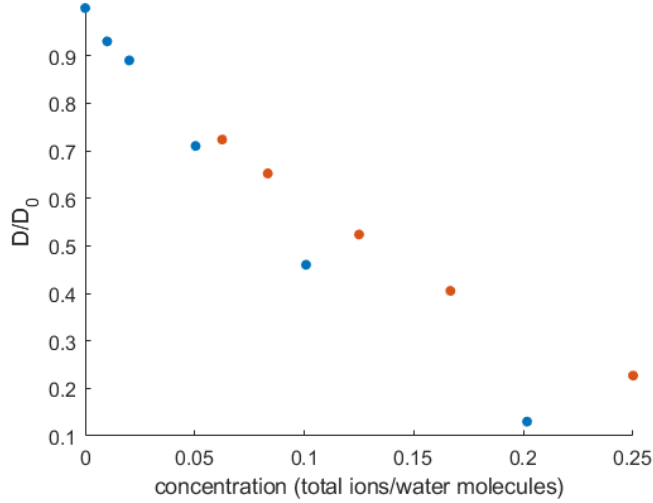


Figure 3.22: Diffusion coefficient of water in solution divided by value in pure water in bulk from literature (blue) and in films from simulation (red) at various concentrations. For simulation, interval length was 100 ps and averages were taken over 99 measurements.

Subsequently, the diffusion of the ions themselves was measured. The results are shown in Figure 3.23.

From the Stokes-Einstein equation it is expected that the diffusivity of particles is inversely proportional to their radii,

$$D \sim \frac{1}{r}.$$

If we take the Lennard-Jones σ values as radii, we would expect

$$D_{Cl}/D_{Li} = \sigma_{Li}/\sigma_{Cl} = \frac{1.41}{4.83} = 0.29.$$

However, the measurements show that chloride ions are more diffusive than lithium ions. The ratios of the diffusion coefficients of chloride and lithium ions were calculated and are given in Table 3.4. These suggest that $D_{Cl}/D_{Li} = 1.3$ with the value of the water films containing 256 waters as an outlier.

Table 3.4: Diffusion coefficients of Cl and Li and their ratio

water count	total ions/water	D_{xyCl} (10^{-9} m 2 /s)	D_{xyLi} (10^{-9} m 2 /s)	D_{Cl}/D_{Li}
256	1/4	0.140	0.123	1.14
384	1/6	0.346	0.275	1.26
512	1/8	0.573	0.438	1.31
768	1/12	0.913	0.682	1.34
1024	1/16	1.078	0.828	1.30

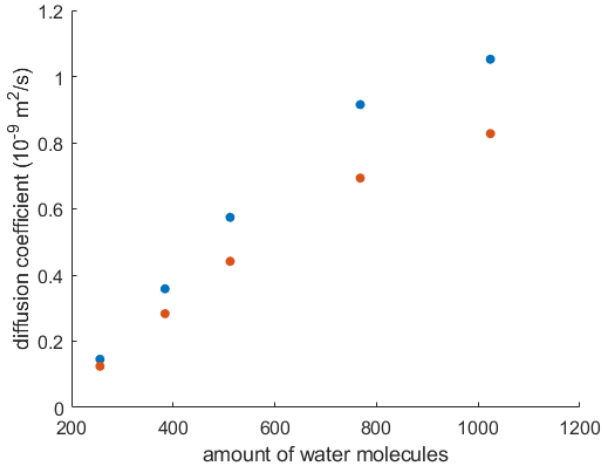


Figure 3.23: *Diffusion coefficient D_x of dissolved chloride (blue) and lithium ions (red) for various amounts of water. Interval length was 100 ps, averages were taken over 99 measurements.*

The U.S. Geological Society [46] states diffusion coefficients of $2.03 \cdot 10^{-9} \text{ m}^2/\text{s}$ for chloride and $1.03 \cdot 10^{-9} \text{ m}^2/\text{s}$ for lithium ions, as can be read on the website of Aqion [47]. This agrees with the higher diffusivity for chloride.

Nightingale [48] proposed the use of hydrated radii of ions and found values of 3.82 Å for lithium and 3.32 Å for chloride. From this $D_{Cl}/D_{Li} = 1.15$ would be expected, which is in better agreement with the value of 1.3 found from the simulations. We can therefore conclude that the diffusion of these ions depends on their effective hydrated radii and not on the radii of only the ions themselves.

Chapter 4

Conclusions and Outlook

4.1 Conclusions

ThermoChemical Materials (TCMs) can be used in heat batteries for seasonal heat storage. Salt hydrates are TCMs that are well-suited for use in housing. The hydration process in these salts is exothermic and the battery can be charged by heating and thereby dehydrating the material. Experimental studies suggest that the transition from anhydrous salt to a hydrate takes place with an intermediate step, dissolution into a thin film of water.

In this thesis, the salt hydrate lithium chloride has been investigated using atomistic molecular-dynamics computer simulations. The goal of this thesis was to provide in-depth information on the dissolution process of lithium chloride on the atomic scale.

Force field data were taken from literature and benchmarked. Subsequently, simulations of the interactions of water films with anhydrous LiCl were analysed.

The following conclusions were drawn:

The self-diffusion of water in films on the surface of LiCl crystals increases with the amount of water. Water molecules are slowed down when they are near the salt surface. In thicker films, the diffusion coefficient approaches its bulk value.

Water molecules at the crystal surface have a preferred orientation, with the oxygen atom being closest to the surface and near a lithium ion. Because lithium ions are smaller than chloride ions, water molecules can approach the lithium closer and the minimum of potential energy is lower. This preferential orientation was most clearly observed for the water molecules present in the primary density peak.

The time needed to dissolve ions depends on the surface geometry of the salt. On flat surfaces, no dissolution was observed within 50 ns. The extrusions in a Stub system dissolved fastest since ions on corners are not strongly bound and easily approachable. Ridge and Dent systems showed slower dissolution, slowest for Dent.

The time needed to dissolve ions decreases with the amount of water in the films. In films with fewer than 512 water molecules, the time at which the first chloride ion dissolves decreases fast with increasing amount of water. At higher amounts of water per film, the decrease in time until first chloride dissolution is smaller. For lithium ions, no such relation was observed.

The occupancy of hydration shells changes with the total amount of water. In films with 384 and 256 water molecules per film, with in total 64 dissolved ions per film, the occupancy decreased with the amount of water. Films with 512 and 768 water molecules had equal occupancy of the hydration shells.

Self-diffusion of water is lowered by the presence of ions in the water film. The relation between ion concentration and water diffusion is linear.

By studying all these aspects of the dissolution process at once, insight was obtained on deliquescence of lithium chloride. Dissolution of LiCl into thin films as a function of the amount of water in the films had not previously been investigated.

Simulation of the full hydration process is not possible with MD because the time-scale of this process is larger than what is accessible with MD. Due to the approximative character of the force fields, MD cannot give accurate results for both solids and solutions with the same force field. However, much insight into the dynamics of the dissolution process was gained, which is the strength of MD.

From our observations, we see a positive effect of the amount of water molecules per film on the mobility of the water and on the speed of the dissolution process. We therefore hypothesise that higher water vapour pressure results in faster hydration of the salt.

4.2 Outlook

In this thesis, the formation of water films by attraction of water vapour to the salt surface was not studied by itself. More information can be obtained on the formation of the water films and on the influence this has on dissolution. A topic of interest here is the transition of "islands" at low amounts of water to smoother films when more water is present.

Chloride ions were observed to dissolve easier than lithium ions. This preference for the first dissolved ion to be chloride was not studied in detail. By analysing the dissolution of single ions, for example on how many water molecules are interacting with an ion during dissolution, better understanding can be gained.

To learn more about the hydration process as a whole, it would be useful to look into the second step, recrystallisation. This can be studied with MD by starting with a solution of salt and slowly, randomly removing water molecules, thereby bringing the concentration to the precipitation value.

Dehydration should also be studied to get a full understanding of the working principles of heat batteries containing this salt hydrate. To be able to simulate this, first planes in the monohydrated crystal that are electrically neutral have to be searched for. These planes can then function as outer planes of the crystal. Furthermore, it might be needed to start simulations at lower temperatures than room temperature and to have some water vapour present near the crystal instead of completely empty space.

The force fields used in this study are optimised for solutions. It is therefore questionable if dehydration of the monohydrate crystal can be simulated using the same force fields. To construct suitable models, Density Functional Theory (DFT) can be used.

Within the time-scale of molecular-dynamics, a full hydration process cannot be simulated with reasonable computational resources. This can be achieved by using coarse-grained models, which does provide less detailed information than MD however.

For another salt hydrate of interest, potassium carbonate, very few data are available in literature. To study this material, a multi-scale approach is recommended:

First, the anhydrous and hydrated crystal can be modelled using DFT. When the crystal dimensions and energies agree with experimental values, the structure of water films on the anhydrous salt can be studied precisely.

The DFT force fields can then be used to construct force fields for classical MD. With classical MD, the dynamics of multiple parts of the hydration and dehydration processes can subsequently be elaborately studied.

Finally, the full (de)hydration process of larger crystals can be studied by use of coarse-grained simulations, which can give insight in phenomena like porosity which take place on much larger length-scales.

Bibliography

- [1] L. C. Sögütoglu, P. A. Donkers, H. R. Fischer, H. P. Huinink, and O. C. Adan, “In-depth investigation of thermochemical performance in a heat battery: Cyclic analysis of K_2CO_3 , $MgCl_2$ and Na_2S ,” *Applied Energy*, vol. 215, no. January, pp. 159–173, 2018.
- [2] Sotherco, “Compact Solar Thermochemical Energy Storage,” http://www.sotherco.eu/en/index_en.html date accessed: 10-10-2019, 2017.
- [3] K. E. N'Tsoukpoe, H. Liu, N. Le Pierrès, and L. Luo, “A review on long-term sorption solar energy storage,” *Renewable and Sustainable Energy Reviews*, vol. 13, no. 9, pp. 2385–2396, 2009.
- [4] P. A. Donkers, L. C. Sögütoglu, H. P. Huinink, H. R. Fischer, and O. C. Adan, “A review of salt hydrates for seasonal heat storage in domestic applications,” *Applied Energy*, vol. 199, pp. 45–68, 2017.
- [5] TNO, “Een warmtebatterij voor thuis: compact, stabiel, betaalbaar,” <https://www.tno.nl/nl/tno-insights/artikelen/een-warmtebatterij-voor-in-huis-compact-stabiel-en-betaalbaar/> date accessed: 10-10-2019, 2019.
- [6] H. P. Huinink and D. Zahn, “Elucidating water dynamics in $MgCl_2$ hydrates from molecular dynamics simulation,” *Solid State Sciences*, vol. 69, pp. 64–70, 2017.
- [7] L. C. Sögütoglu, M. Steiger, J. Houben, D. Biemans, H. R. Fischer, P. Donkers, H. Huinink, and O. C. Adan, “Understanding the Hydration Process of Salts: The Impact of a Nucleation Barrier,” *Crystal Growth and Design*, vol. 19, no. 4, pp. 2279–2288, 2019.
- [8] W. Humphrey, A. Dalke, and K. Schulten, “VMD: Visual Molecular Dynamics,” *Journal of Molecular Graphics*, vol. 14, no. 1, pp. 33–38, 1996.
- [9] R. Bahadur, L. M. Russell, S. Alavi, S. T. Martin, and P. R. Buseck, “Void-induced dissolution in molecular dynamics simulations of $NaCl$ and water,” *Journal of Chemical Physics*, vol. 124, no. 15, 2006.
- [10] L. M. Liu, M. Krack, and A. Michaelides, “Interfacial water: A first principles molecular dynamics study of a nanoscale water film on salt,” *Journal of Chemical Physics*, vol. 130, no. 23, 2009.
- [11] M. C. Foster and G. E. Ewing, “Adsorption of water on the $NaCl(001)$ surface. II. An infrared study at ambient temperatures,” *Journal of Chemical Physics*, vol. 112, no. 15, pp. 6817–6826, 2000.
- [12] D. A. Bruzewicz, A. Checco, B. M. Ocko, E. R. Lewis, R. L. McGraw, and S. E. Schwartz, “Reversible uptake of water on $NaCl$ nanoparticles at relative humidity below deliquescence point observed by noncontact environmental atomic force microscopy,” *Journal of Chemical Physics*, vol. 134, no. 4, 2011.

BIBLIOGRAPHY

- [13] F. Moučka, M. Lísal, and W. R. Smith, “Molecular simulation of aqueous electrolyte solubility. 3. alkali-halide salts and their mixtures in water and in hydrochloric acid,” *Journal of Physical Chemistry B*, vol. 116, no. 18, pp. 5468–5478, 2012.
- [14] K. Heinzinger and P. C. Vogel, “A Molecular Dynamics Study of Aqueous Solutions III. A Comparison of Selected Alkali Halides,” *Zeitschrift fur Naturforschung - Section A Journal of Physical Sciences*, vol. 31, no. 5, pp. 463–475, 1976.
- [15] N. Fukushima, Y. Tamura, and H. Ohtaki, “Dissolution of Alkali Fluoride and Chloride Crystals in Water Studied by Molecular Dynamics Simulations,” *Zeitschrift fur Naturforschung - Section A Journal of Physical Sciences*, vol. 46, pp. 193 – 202, 1991.
- [16] H. Du and J. D. Miller, “Interfacial water structure and surface charge of selected alkali chloride salt crystals in saturated solutions: A molecular dynamics modeling study,” *Journal of Physical Chemistry C*, vol. 111, no. 27, pp. 10013–10022, 2007.
- [17] B. Downs, R. Swaminathan, and K. Bartelmehs, “American Mineralogist Crystal Structure Database,” <http://rruff.geo.arizona.edu/AMSCSD.php>, 1993.
- [18] R. Wyckoff, *Crystal Structures*. New York, London, Sydney: Interscience Publishers, 2nd ed., 1964.
- [19] P. Jeffrey, “X-ray Data Collection Course,” <http://xray0.princeton.edu/%7Ephil/Facility/Guides/XrayDataCollection.html> date accessed: 18-03-2020, 2006.
- [20] N. L. Sandia, “LAMMPS Molecular Dynamics Simulator,” <https://lammps.sandia.gov/>, 2020.
- [21] L. Verlet, “Computer ”experiments” on classical fluids. I. Thermodynamical properties of Lennard-Jones molecules,” *Physical Review*, vol. 159, no. 1, pp. 98–103, 1967.
- [22] M. P. Allen and D. J. Tildesley, *Computer Simulation of Liquids*. Oxford University Press, 2017.
- [23] D. Frenkel and B. Smit, *Understanding Molecular Simulation*. Academic Press, 1996.
- [24] W. Shinoda, M. Shiga, and M. Mikami, “Rapid estimation of elastic constants by molecular dynamics simulation under constant stress,” *Physical Review B - Condensed Matter and Materials Physics*, vol. 69, no. 13, pp. 16–18, 2004.
- [25] M. E. Tuckerman, J. Alejandre, R. López-Rendón, A. L. Jochim, and G. J. Martyna, “A Liouville-operator derived measure-preserving integrator for molecular dynamics simulations in the isothermal-isobaric ensemble,” *Journal of Physics A: Mathematical and General*, vol. 39, no. 19, pp. 5629–5651, 2006.
- [26] A. Parrinello, M.; Rahman, “Crystal Structure and Pair Potentials: A Molecular-Dynamics Study,” *Physical Review Letters*, vol. 45, no. 14, pp. 1196–1199, 1980.
- [27] J. Lennard-Jones and A. Devonshire, “The Interaction of Atoms and Molecules with Solid Surfaces . VII . The Diffraction of Atoms by a Surface,” *Proceedings of the Royal Society of London. Series A, Mathematical and Physical Sciences*, vol. 158, no. 894, pp. 253–268, 1937.
- [28] P. P. Ewald, “Die Berechnung optischer und elektrostatischer Gitterpotentiale,” *Annalen der Physik*, vol. 369, no. 3, pp. 253–287, 1921.
- [29] E. L. Pollock and J. Glosli, “Comments on P3M, FMM, and the Ewald method for large periodic Coulombic systems,” *Computer Physics Communications*, vol. 95, no. 2-3, pp. 93–110, 1996.

- [30] H. J. Berendsen, J. R. Grigera, and T. P. Straatsma, “The missing term in effective pair potentials,” *Journal of Physical Chemistry*, vol. 91, no. 24, pp. 6269–6271, 1987.
- [31] W. L. Jorgensen, “Transferable Intermolecular Potential Functions for Water, Alcohols, and Ethers. Application to Liquid Water,” *Journal of the American Chemical Society*, vol. 103, no. 2, pp. 335–340, 1981.
- [32] H. W. Horn, W. C. Swope, J. W. Pitera, J. D. Madura, T. J. Dick, G. L. Hura, and T. Head-Gordon, “Development of an improved four-site water model for biomolecular simulations: TIP4P-Ew,” *Journal of Chemical Physics*, vol. 120, no. 20, pp. 9665–9678, 2004.
- [33] Sandia, “SPC water model - LAMMPS documentation,” https://lammps.sandia.gov/doc/Howto_spc.html date accessed: 31-03-2020, 2020.
- [34] J. P. Ryckaert, G. Ciccotti, and H. J. Berendsen, “Numerical integration of the cartesian equations of motion of a system with constraints: molecular dynamics of n-alkanes,” *Journal of Computational Physics*, vol. 23, no. 3, pp. 327–341, 1977.
- [35] D. Chandler, *Introduction to Statistical Mechanics*. Oxford University Press, 1987.
- [36] A. Kohlmeyer, “Unexpected out of range atoms error with pppm/tip4p and triclinic boxes,” <https://github.com/lammps/lammps/issues/869>, 2018.
- [37] H. Shinto, T. Sakakibara, and K. Higashitani, “Molecular dynamics simulations of water at NaCl(001) and NaCl(011) surfaces,” *Journal of Physical Chemistry B*, vol. 102, no. 11, pp. 1974–1981, 1998.
- [38] Q. Dai, J. Hu, and M. Salmeron, “Adsorption of water on NaCl (100) surfaces: Role of atomic steps,” *Journal of Physical Chemistry B*, vol. 101, no. 11, pp. 1994–1998, 1997.
- [39] G. Lanaro and G. N. Patey, “Molecular dynamics simulation of nacl dissolution,” *Journal of Physical Chemistry B*, vol. 119, no. 11, pp. 4275–4283, 2015.
- [40] Y. Yang, S. Meng, and E. G. Wang, “A molecular dynamics study of hydration and dissolution of NaCl nanocrystal in liquid water,” *Journal of Physics Condensed Matter*, vol. 18, no. 45, pp. 10165–10177, 2006.
- [41] L. M. Liu, A. Laio, and A. Michaelides, “Initial stages of salt crystal dissolution determined with ab initio molecular dynamics,” *Physical Chemistry Chemical Physics*, vol. 13, no. 29, pp. 13162–13166, 2011.
- [42] E. Oyen and R. Hentschke, “Molecular dynamics simulation of aqueous sodium chloride solution at the NaCl(001) interface with a polarizable water model,” *Langmuir*, vol. 18, no. 2, pp. 547–556, 2002.
- [43] S. Garcia-Manyes, A. Verdaguer, P. Gorostiza, and F. Sanz, “Alkali halide nanocrystal growth and etching studied by AFM and modeled by MD simulations,” *Journal of Chemical Physics*, vol. 120, no. 6, pp. 2963–2971, 2004.
- [44] P. Jungwirth, “How Many Waters Are Necessary to Dissolve a Rock Salt Molecule?,” *Journal of Physical Chemistry A*, vol. 104, no. 1, pp. 145–148, 2000.
- [45] D. W. McCall and D. C. Douglass, “The effect of ions on the self-diffusion of water. I. Concentration dependence,” *Journal of Physical Chemistry*, vol. 69, no. 6, pp. 2001–2011, 1965.
- [46] U. S. Geological Society, “PHREEQC,” <https://www.usgs.gov/software/phreeqc-version-3> date accessed: 26-03-2020, 2020.
- [47] H. Kalka, “Aqion,” <https://www.aqion.de/site/194> date accessed: 25-03-2020, 2015.

BIBLIOGRAPHY

- [48] E. R. Nightingale, “Phenomenological theory of ion solvation. Effective radii of hydrated ions,” *Journal of Physical Chemistry*, vol. 63, no. 9, pp. 1381–1387, 1959.

Appendix A

Appendices

A.1 Input parameters available from literature

Apart from the SPC/e water model and the corresponding Lennard-Jones parameters, also the TIP3P and TIP4P-Ew water models with their respective LJ parameters were benchmarked, as described in Section 3.1. These data were taken from the article by Moucka et al. [13].

Table A.1: LJ parameters, partial charges and masses per atom type used with the TIP3P water model [13]

	ϵ (kJ/mol)	σ (Å)	q (e)	m (g/mol)
Li	0.12	1.83	+1	6.941
Cl	0.15	4.48	-1	35.453
H	0.000	0.000	+0.417	1.00794
O	0.1521	3.1506	-0.834	15.9994

Table A.2: Parameter values of the harmonic bond and angle potentials for the TIP3P water model [30][33]

K_a (kJ/mol)	230
K_b (kJ/(mol·Å ²))	1883
θ_0 (degrees)	104.52
r_0 (Å)	0.9572

Table A.3: LJ parameters, partial charges and masses per atom type used with the TIP4P-Ew water model [13]

	ϵ (kJ/mol)	σ (Å)	q (e)	m (g/mol)
Li	0.42	1.44	+1	6.941
Cl	0.050	4.92	-1	35.453
H	0.000	0.000	+0.5242	1.00794
O	0.6811	3.164	-1.0484	15.9994

Table A.4: Parameter values of the harmonic bond and angle potentials for the TIP4P-Ew water model [30][33]

K_a (kJ/mol)	4184
K_b (kJ/(mol·Å ²))	418
θ_0 (degrees)	104.52
r_0 (Å)	0.9572

A.2 Water adding

Water was initially added by using the *deposit* function of LAMMPS. However, for some systems the formation of a smooth water film took so long that ions were going into dissolution before the film formation was complete. Also, the film sometimes had not fully come to rest yet while the potential energy was already stable, as can be seen here for the Stub system:

Table A.5: Times after which the potential energy (t_E) and the film thickness (t_{film}) were stable and at which the first ions of Li and Cl went into solution in a Stub system with 256 water molecules per film

Waters	t_E (ps)	t_{film} (ps)	t_{Li} (ps)	t_{Cl} (ps)
64	150	200	30	not within 1 ns
128	350	500	200	80
192	300	not within 1ns	650	80
256	200	600	630	30
384	200	200	210	50
512	200	200	330	30
768	100	200	10	40
1024	100	100	190	40

Another method was therefore used, as described in Section 2.6.

A.3 Additional measurements of dissolution

A.3.1 Dissolution quantified for different geometries into a film with 512 water molecules

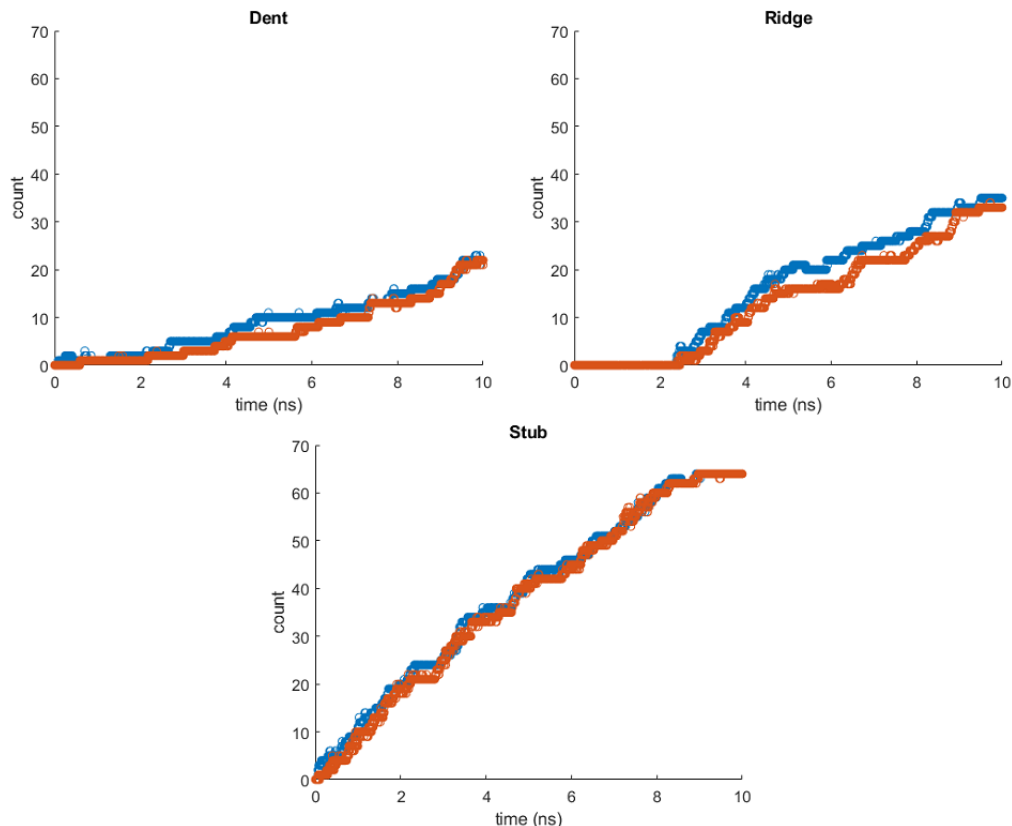


Figure A.1: *Dissolved ion counts for Dent, Ridge and Stub. Chloride in blue, lithium in red. Water films contain 512 water molecules.*

A.3.2 Dissolution visualised for different geometries into a film with 512 water molecules

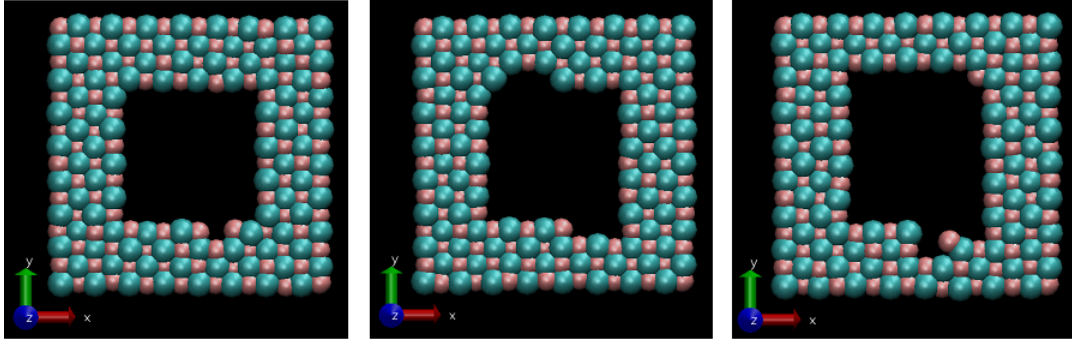


Figure A.2: *Dissolution process of a dent, $t = 2134, 4016$ and 5777 ps. Cl blue, Li red. Films contain 512 water molecules. Chloride dissolves easier than lithium. Dissolution usually starts near corners.*

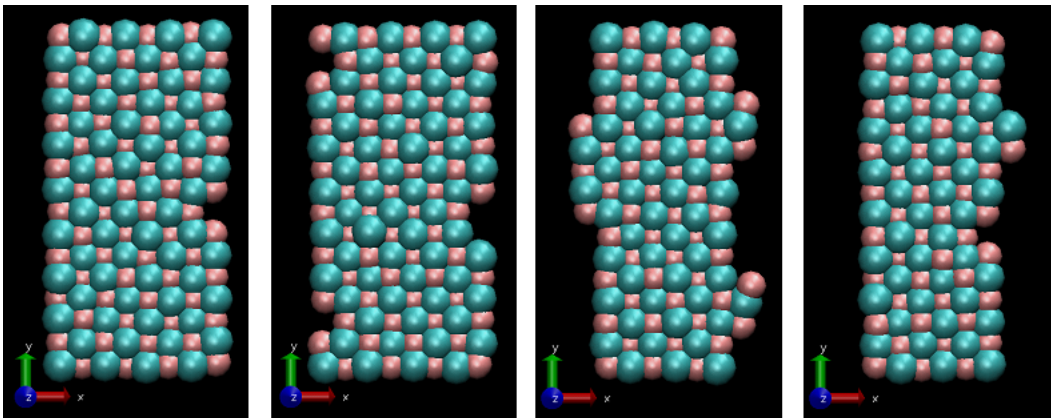


Figure A.3: *Dissolution process of a ridge, $t = 2472, 2882, 5994$ and 9273 ps. Cl blue, Li red. Films contain 512 water molecules. Chloride dissolves easier than lithium. New (partial) rows start dissolving before previous ones are fully dissolved.*

A.4 LAMMPS input file

The following example of a LAMMPS input file was used to simulate an equilibrated Stub system for 1 ns:

```

units real
atom_style full

processors * * 1

read_restart restart.stub1ns

pair_style lj/cut/coul/long 11.0 11.0
kspace_style pppm 1.0e-4

bond_style harmonic
angle_style harmonic
dihedral_style none
improper_style none

bond_coeff 1 1000.00 1.000
angle_coeff 1 100.0 109.47

special_bonds    lj/coul 0.0 0.0 0.5

pair_coeff 1 1  0.3367  1.41
pair_coeff 2 2  0.01278 4.83
pair_coeff * 3  0.0000  0.0000
pair_coeff 4 4  0.15535 3.166

pair_modify mix arithmetic

neighbor 2.0 bin
neigh_modify every 1 delay 0 check yes

dump id all xyz 1000 dump.xyz
dump_modify id element Li Cl H O

compute moved all displace/atom

dump many all custom 1000 many.*.txt id type x y z xu yu zu c_moved[*]

thermo_style custom step time cpu temp press pe ke evdw ecoul elong
cella cellb cellc cellalpha cellbeta cellgamma
thermo 500

region cube block 20 22 20 22 20 22 units box

group salt region cube

fix still salt momentum 1 linear 1 1 1

fix 1 all shake 0.0001 20 0 b 1 a 1

```

APPENDIX A. APPENDICES

```
fix 2 all nvt temp 300.0 300.0 100.0

group crystal type 1 2
group water type 4

compute msdstill salt msd
fix msdstill salt ave/time 1 1 1000 c_msdstill[*] file salt.msd

compute msdcrystal crystal msd
fix msdcrystal crystal ave/time 1 1 1000 c_msdcrystal[*] file crystal.msd

compute msdwater water msd
fix msdwater water ave/time 1 1 1000 c_msdwater[*] file water.msd

run 1000000

write_data data.stubrun1ns
write_restart restart.stubrun1ns
```

A.5 MATLAB scripts

A.5.1 Import script

The following script was used to import the data from the *many.*.txt* files dumped by LAMMPS. Here '*' was replaced by the timestep at which the data was dumped. This seemingly cumbersome method made sure that all files could be correctly loaded into MATLAB.

```
%% Import data from text file.

% Auto-generated by MATLAB on 2019/11/01 16:32:39
% Edited to load multiple files, placing data in a 3D array

for k = 1:1000
    %% Initialize variables.
    filename = sprintf('many.%d.txt',k*1000+2201000);
    delimiter = ' ';
    startRow = 10;

    %% Format for each line of text:
    % column1: double (%f)
    % column2: double (%f)
    % column3: double (%f)
    % column4: double (%f)
    % column5: double (%f)
    % column6: double (%f)
    % column7: double (%f)
    % column8: double (%f)
    % column9: double (%f)
    % column10: double (%f)
    % column11: double (%f)
    % column12: double (%f)
    % For more information, see the TEXTSCAN documentation.
    formatSpec = '%f%f%f%f%f%f%f%f*f%*s%[^\\n\\r]';

    %% Open the text file.
    fileID = fopen(filename,'r');

    %% Read columns of data according to the format.
    % This call is based on the structure of the file used to generate this
    % code. If an error occurs for a different file, try regenerating the code
    % from the Import Tool.
    dataArray = textscan(fileID, formatSpec, 'Delimiter', delimiter,
        'MultipleDelimsAsOne', true, 'TextType', 'string', 'EmptyValue',
        NaN, 'HeaderLines', startRow-1, 'ReturnOnError', false,
        'EndOfLine', '\r\n');

    %% Close the text file.
    fclose(fileID);

    %% Post processing for unimportable data.
    % No unimportable data rules were applied during the import, so no post
```

```
% processing code is included. To generate code which works for
% unimportable data, select unimportable cells in a file and regenerate the
% script.

%% Create output variable

temp = [dataArray{1:end-1}];
sorted = sortrows(temp);
many(:,:,k) = sorted(:,:,k);

%% Clear temporary variables
clearvars filename delimiter startRow formatSpec fileID dataArray ans;
end
```

A.5.2 Script to Measure Orientation of Water Molecules

To calculate angles of water molecules with the z-axis, the following script was used:

```
time=1000;
water = zeros(128,10,time);
toptot=zeros(1,1);
bottomtot=zeros(1,1);
for t=1:time
    j=1;
    k=1;
    l=1;
    for i=1:length(many)
        % scan all atoms

        if many(i,2,t) == 4
            % search for the oxygen atoms

            water(j,1,t) = (many(i+1,6,t) + many(i+2,6,t))/2;
            water(j,2,t) = (many(i+1,7,t) + many(i+2,7,t))/2;
            water(j,3,t) = (many(i+1,8,t) + many(i+2,8,t))/2;
            % calculate the position of the centre between the hydrogen
            % atoms of this molecule, unwrapped coordinates

            water(j,4,t) = many(i,8,t);
            % take the Z-coordinate of the oxygen atom

            water(j,5,t) = water(j,3,t) - water(j,4,t);
            % take the difference in Z of the hydrogens' centre and the oxygen

            water(j,6,t) = sqrt((water(j,1,t) - many(i,6,t))^2 +
            (water(j,2,t) - many(i,7,t))^2);
            % calculate the distance of the hydrogens' centre to the oxygen
            % projected on the XY-plane

            water(j,7,t) = sqrt(water(j,5,t)^2 + water(j,6,t)^2);
            % calculate the hypotenuse of the triangle formed by the H-centre,
            % O and projection of O on the same XY-plane as H-centre
```

```
water(j,8,t) = acos(water(j,5,t)/water(j,7,t));
% calculate the angle with z-axis using inverse cosine

water(j,9,t) = many(i,5,t);
if water(j,9,t) > 40
    top(k,1,t) = water(j,8,t)/pi;
    k = k+1;
else
    bottom(l,1,t) = water(j,8,t)/pi;
    l = l+1;
end
% save the angle [pi radians] in an array for either the top film or
the bottom film

j = j+1;
end
end
toptot=cat(1,toptot,top(:,1,t));
bottomtot=cat(1,bottomtot,bottom(:,1,t));
% concatenate measurements from all timesteps into a single vector
end
```